Peer-reviewed version available at *Cancers* **2020**, *12*, 1260; doi:10.3390/cancers12051260

Article

Knockout of MMP3 Weakened Solid Tumor Organoids and Cancer Extracellular Vesicles

Eman A. Taha[1,2,3], Chiharu Sogawa[1], Yuka Okusha[1,4], Hotaka Kawai[5], May Wathone Oo[5], Abdellatif El-Seoudi[6,7], Yanyin Lu[1,8], Hitoshi Nagatsuka[5], Satoshi Kubota[8], Ayano Satoh[2], Kuniaki Okamoto[1] and Takanori Eguchi[1,9,*]

[1] Department of Dental Pharmacology, Okayama University Graduate School of Medicine, Dentistry and Pharmaceutical Sciences, Okayama 700-8525, Japan.
[2] Department of Medical Bioengineering, Okayama University Graduate School of Natural Science and Technology, Okayama 700-8530, Japan.
[3] Department of Biochemistry, Ain Shams University Faculty of Science, Cairo 11566, Egypt.
[4] Division of Molecular and Cellular Biology, Department of Radiation Oncology, Beth Israel Deaconess Medical Center, Harvard Medical School, Boston, MA 02115, USA.
[5] Department of Oral Pathology and Medicine, Okayama University Graduate School of Medicine, Dentistry and Pharmaceutical Sciences, Okayama 700-8525, Japan.
[6] Department of Biochemistry and Molecular Dentistry, Okayama University Graduate School of Medicine, Dentistry and Pharmaceutical Sciences, Okayama 700-8525, Japan.
[7] Centre Hospitalier Universitaire Sainte-Justine Hospital Research Center, University of Montreal, Québec H3T 1C5, Canada.
[8] Department of Dental Anesthesiology, Okayama University Graduate School of Medicine, Dentistry and Pharmaceutical Sciences, Okayama 700-8525, Japan.
[9] Advanced Research Center for Oral and Craniofacial Sciences, Okayama University Graduate School of Medicine, Dentistry and Pharmaceutical Sciences, Okayama 700-8525, Japan.
* Correspondence: eguchi@okayama-u.ac.jp eguchi.takanori@gmail.com

Abstract: The tumor organoid (tumoroid) model in three-dimensional (3D) culture systems has been developed to reflect more closely the in vivo tumors than 2D-cultured tumor cells. Notably, extracellular vesicles (EVs) are efficiently collectible from the culture supernatant of gel-free tumoroids. Matrix metalloproteinase (MMP) 3 is a multi-functional factor playing crucial roles in tumor progression. However, roles of MMP3 within tumor growth and EVs have not unveiled. Here, we investigated the protumorigenic roles of MMP3 on integrities of tumoroids and EVs. We generated MMP3-knockout (KO) cells using the CRISPR/Cas9 system from rapidly metastatic LuM1 tumor cells. Moreover, we established fluorescent cell lines with palmitoylation signal-fused fluorescent proteins (tdTomato and enhanced GFP). Then we confirmed the exchange of EVs between cellular populations and tumoroids. LuM1-tumoroids released large EVs (300-1000 nm) and small EVs (50-200 nm) while the knockout of MMP3 resulted in the additional release of broken EVs from tumoroids. The loss of MMP3 led to a significant reduction in tumoroid size and to the development of the necrotic area within tumoroids. MMP3 and CD9 (a category-1 EV marker tetraspanin protein) were significantly down-regulated in MMP3-KO cells and their EV fraction. These weakened phenotypes by MMP3 KO were markedly rescued by the addition of MMP3-rich EVs or conditioned medium (CM) collected from LuM1-tumoroids, which caused a dramatic rise in the expression of MMP3, CD9, and Ki-67 (a marker of proliferating cells) in the MMP3-null/CD9-low tumoroids. Notably, MMP3 enriched in tumoroids-derived EVs and CM deeply penetrated into recipient MMP3-KO tumoroids, resulting in a remarkable enlargement of solid tumoroids, while MMP3-null EVs did not. These data

demonstrate that EVs can mediate molecular transfer of MMP3 resulting in increasing the proliferation and tumorigenesis, indicating crucial roles of MMP3 in tumor progression.

Keywords: Matrix metalloproteinase 3 (MMP3); extracellular vesicles (EVs); tumoroid; tumor organoid, tumorigenesis, three-dimensional (3D) culture system

Introduction

Extracellular vesicles (EVs) are lipid bi-layered vesicles released from cells under physiological and pathological conditions. EVs are key players in intercellular communications at local and distant sites [1]. EVs carry various molecular cargos such as nucleic acids, proteins, lipids and metabolites [1]–[4]. Small EVs (s-EVs) often include exosomes secreted via exocytosis and ectosomes (aka microvesicles or microparticles) released from cellular membrane budding and shedding. Additionally, large EVs (L-EVs) have been reported [5]–[9].Of note**,** EVs are heterogeneous populations, so there is no unanimous consensus on the nomenclature of them. General terms such as "exosomes" and "microvesicles" have been broadly used. The International Society for Extracellular Vesicles (ISEV) proposed to use the term EVs in general to describe vesicles naturally released from the cells and surrounded by a lipid bilayer [10]. In the present study, we will use the term EVs in general and classify them into s-EVs and L-EVs based on the size of vesicles. Notably, tumor-derived EVs can reprogram the recipient cells by transferring their bioactive cargo into them [8], [11], [12]. In the present study, we aimed to explore the roles of tumor-derived EVs in tumor development *in vitro*.

The matrix metalloproteinase (MMP) family consists of about 28 members that share similarities in their structure, regulation, and function [13]. All MMPs have three principal domains; (1) a pro-domain that functions as an intramolecular inhibitor to maintain the enzyme in an. inactive state, (2) a catalytic domain that promotes the proteolytic activity, and (3) a hemopexin-like repeat domain (PEX), which determines the substrate specificity [14]–[18]. Earlier studies showed that MMPs constituted a large family of zinc/calcium-dependent endopeptidases and were considered as the main players in extracellular matrix (ECM) remodeling due to their ability to degrade numerous components of ECM and non-ECM proteins, such as adhesion molecules, cytokines, protease inhibitors, and membrane receptors (Berg et al., 2019). Later studies have shown that matrix metalloproteinase 3 (MMP3) was a bifunctional protein that acts as a proteolytic enzyme and a transcriptional factor, playing crucial roles in tumor progression [19]–[21]. Therefore, we defined MMP3 as a moonlighting protein as it plays multiple roles in the cells as a proteinase as well as a transcription factor [22]. It has been shown that some members of MMPs were expressed at high levels in particular cancer types and promoted tumor progression. We have compared protumorigenic phenotypes of rapidly metastatic murine cancer cell line LuM1 with a parental cancer cell line Colon26 (aka CT26) [20], [21], [23]–[25] and shown that MMP3 and MMP9 were highly expressed in LuM1 cells. The RNA interference (RNAi)-mediated knockdown of MMP3 and MMP9 significantly attenuated tumor growth and metastasis in the allograft mouse model [21]. Most recently, we established MMP3-knockout (KO) cells using CRISPR/Cas9 genome editing technology on the LuM1 cells and then compared the oncogenic effects of MMP3-KO cells versus LuM1 cells *in vivo* and *in vitro* using the 2D culture system [20]. This study indicated that knockout of *Mmp3* results in significant inhibition of tumor growth, cellular migration, and invasion *in vivo* [20]. However, a mechanism of how MMP3 enriched EVs involves characteristics of EVs and tumors has not completed yet. We investigate this issue in the present study.

The two-dimensional (2D) cell cultures have been frequently used for cancer research and drug screening [26]. In conventional 2D cultures, cells are cultured as monolayers on flat surfaces which allows access of the same amount of growth factors and nutrients present in the medium, resulting in homogenous growth and proliferation [27]. Besides, the strong physical interaction presents between cells and 2D substrates resulted in alteration in the tumor cell behaviors that differ from those of tumors growing *in vivo*

[26]. However, the 2D culture model fails to correctly mimic the proper tissue architecture and complex microenvironment of tissues encountered *in vivo* [28]. To overcome limitations of the 2D culture system, a novel 3D cell culture model (aka a spheroid or organoid culture) have been developed to better mimic *in vivo* cell microenvironments [28], [29]. The 3D culture model maintains the interactions between cells and their ECM, and create gradient access of oxygen, nutrient, metabolic wastes buildup, and a combination of tissue-specific scaffolding cells [30]. Similar to human cancers, proliferating, quiescent and dying cells are coexisting in normoxic, hypoxic or necrotic zones within tumor organoids [19], [23], [31]. Thus, the 3D cancer models reflect more closely the *in vivo* human tumors, which prompted us to define tumor organoids as "tumoroids". Among several methodologies of tumoroid models, we have adopted gel-free tumoroid models cultured on NanoCulture Plates (NCP) and ultra-low attachment (ULA) plates [19], [23]–[25], [32]. A big advantage of the gel-free tumoroid model is the collectability of EVs from their culture supernatants. NCP is a nanopatterned gel-free scaffold type 3D cell culture [33]. The mogul field structure on the NCPs restricts cells to sprawl on the base and enable tumor cells to migrate from a scaffold to another scaffold more actively than cells cultured on the 2D plate. The increased migration and lesser attachment of cancer cells on the NCPs enable tumor cells from forming 3D tumoroids or tumoroids [19], [23]–[25], [32]. Besides, ultra-low attachment (ULA) plates have been also useful for the collection of EVs. Cells do not rapidly migrate on ULA plates compared to NCP. Moreover, we have examined a few types of culture media such as serum-containing media versus serum-free stemness-enhancing media in combination with the 3D culture systems. *In vitro* culturing of tumoroids in such a 3D nano-environment combined with a defined stem cell medium enabled the cells to grow slowly and form large organoids that expressed multiple stem cell markers and intercellular adhesion molecules [19], [23]. However, characteristics of EVs derived from 3D tumoroids have not investigated yet. Moreover, roles of tumoroid-derived EVs in tumor development have not unveiled. We therefore investigate these issues in the present study.

Several methods have been developed to monitor the biogenesis, transmission, distribution, and subcellular localization of EVs, such as lipid-based fluorescence labeling [23], [34], such as the transmembrane protein CD63 fused with fluorescent proteins [35], [36] and membrane lipid-binding palmitoylation signal-fused fluorescent proteins such as tandem dimer Tomato (tdTomato) or enhanced green fluorescence protein (EGFP) as we, in the present study, abbreviate as palmGFP (palmG) and palmtdTomato (palmT) [37]. Protein S-acylation is a lipid modification that enables the covalent attachment of long-chain palmitic fatty acids to thiol groups of cysteine residues through a thioester linkage [38], [39]. This type of protein modification is commonly known as S-palmitoylation allows the association of proteins with cellular membranes [40]. The fusion of the fluorescent proteins with palmitoylation sequence to the cell membranes, enabling the whole-cell labeling [41], [42]. As EVs are derived from the plasma membrane [37], we assumed that tagging the plasma membrane with fluorescent proteins would enable the labeling of EVs.

Here, we explored (i) the tumorigenic role of MMP3 on the *in vitro* tumoroid formation under the 3D culture system and on their EVs integrity. We also explored (ii) whether MMP3-rich or MMP3-null EVs could alter tumoroid formation and examined (iii) the EVs-mediated molecular transfer of MMP3 into the MMP3-KO tumoroids under the 3D culture system.

3. Results

3.1. MMP3 knockout impacts physical and biological integrities of extracellular vesicles

To explore the role of MMP3 in the cellular communication in cancer, we used the CRISPR/Cas9 genome editing system for generating MMP3-knockout cell line from a murine high metastatic cancer cell line LuM1 [20]. MMP3 was markedly detected in the cells, non-EVs, and EVs fractions of the LuM1, while the complete

Preprints (www.preprints.org) | NOT PEER-REVIEWED | Posted: 25 March 2020 doi:10.20944/preprints202003.0371.v1

Peer-reviewed version available at Cancers 2020, 12, 1260; doi:10.3390/cancers12051260

loss of MMP3 was confirmed in MMP3-knockout LuM1 cells, non-EVs (e.g. soluble proteins), and EVs fractions (Fig. 1A, top row), suggesting a successful knockout of the *Mmp3* gene. Second, we examined the CD9 tetraspanin (a category-1 EV marker protein) expression pattern. Interestingly, the tetraspanin CD9 content was significantly down-regulated in both cells and EVs fractions of the MMP3-null cells compared to their counterpart (Fig. 1A, second and third rows). The SDS-polyacrylamide gel was stained with CBB after the electrophoretic separation to confirm the loading of protein samples in all lanes (Fig. 1B).

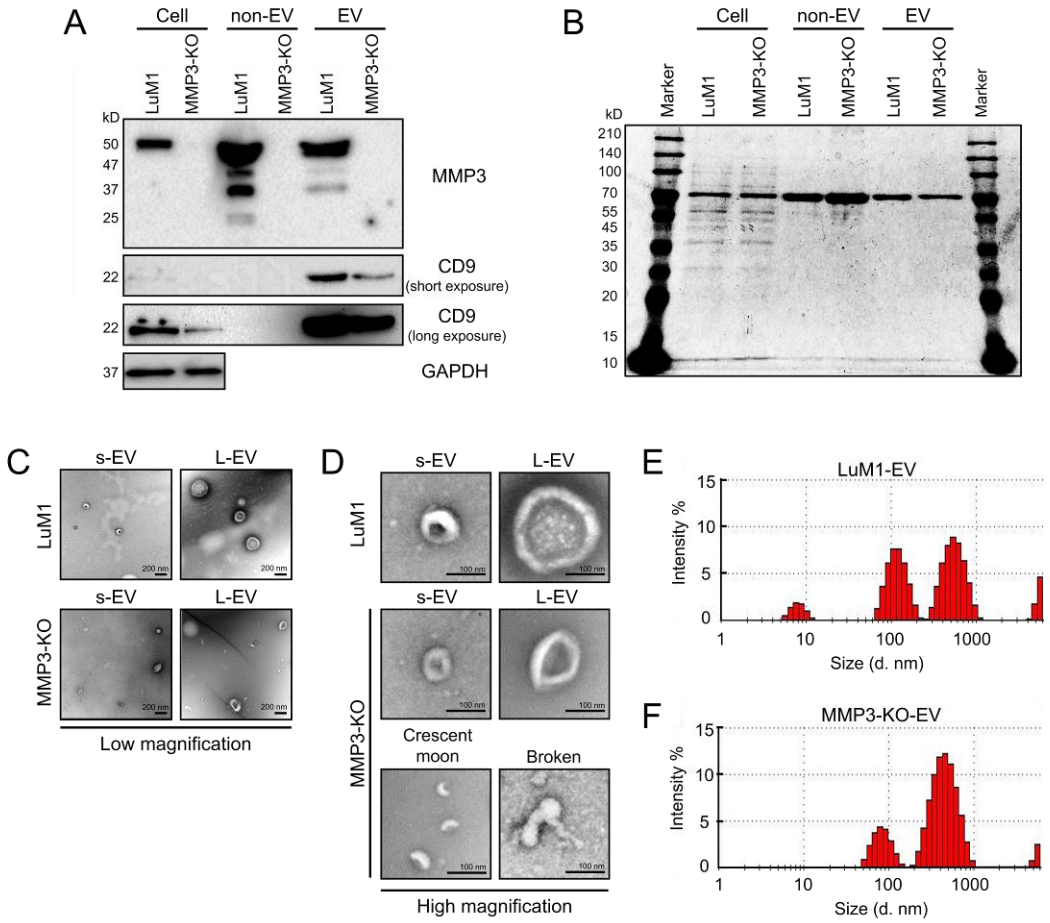

Figure 1: MMP3 knockout impacts physical and biological integrities of extracellular vesicles. Tumoroids were formed in ultra-low attachment (ULA) plates. EV and non-EV fractions were collected from the culture supernatants after 6 days. **(A)** Western blotting showing MMP3, CD9 in tumoroids, non-EVs, and EVs fractions. The 54-kD bands indicate the full-length MMP3, the 47-kD bands represent the active form consists of the catalytic, hinge, and PEX domains, the 37-kD represents the catalytic domain, and the 25-kD shows the PEX domain of MMP3. GAPDH was used as an internal control. **(B)** Coomassie blue staining of the gel indicating the loading of protein samples (1 μg) in all lanes. **(C, D)** TEM images at **(C)** low magnification and (D) high magnification views of EVs derived from the LuM1 and MMP3-KO tumoroids. s-EVs, small EVs; L-EVs, large EVs. Scale bars, 200 nm (in low magnification), and 100 nm (in high magnification). **(E, F)**. Representative histograms showing the particle diameter distributions of EVs derived from the **(E)** LuM1 and **(F)** MMP3-KO tumoroids. The experiments were repeated twice in Figure 1 A-F.

Further, we examined the morphology and size of EVs secreted from "tumoroids" by transmission electron microscopy (TEM) and Zetasizer, respectively. Both LuM1- and MMP3-KO tumoroids released

two types of EVs; small EVs (s-EVs) ranged approximately 50-200 nm and large EVs (L-EVs) showed broad ranges between 200 and 1000 nm (Fig. 1C-F, Table 1). According to their size, the s-EVs were supposed to include exosomes and/or ectosomes (aka microvesicles and microparticles). The size of both s-EVs (peaked at 84 nm) and L-EVs (peaked at 465 nm) released from MMP3-KO tumoroids were smaller than those (peaked at 119 nm and 561 nm, respectively) of LuM1 tumoroids (Fig. 1 E, F). Meanwhile, crescent moon-like shaped and broken EVs were particularly seen in the MMP3-KO EV fraction released by MMP3-KO tumoroids (Fig. 1C, D).

These findings demonstrate that MMP3 is important for maintaining the physical and biological integrities of EVs, and the loss of MMP3 resulted in disorganizing the EVs structures. Besides, MMP3 controls the secretion of CD9-containing EVs.

Table 1. Comparison of particle size distributions between LuM1-EVs and MMP3-KO-EVs.

LuM1-EV				**MMP3-KO-EV**			
Peak	Diameter (nm)	Intensity (%)	Width (nm)	Peak	Diameter (nm)	Intensity (%)	Width (nm)
1	561.4	48.6	164.9	1	464.9	76.6	155.3
2	119.3	38.3	31.8	2	83.9	20.2	20.4
3	8.0	6.8	1.53	3	5374	3.2	326.1
Average: 245.1 nm Polydispersity index (PdI): 0.726, Intercept: 0.886				Average: 277.1 nm Polydispersity index (PdI): 0.647, Intercept: 0.838			

3.2 Loss of Mmp3 reduces the in vitro tumorigenicity.

Next, we examined the consequences of *Mmp3* loss on the *in vitro* tumoroid formation. The LuM1 and MMP3-KO cells were cultured in the 3D culture system either under serum-containing or mTeSR1 stemness-enhancing conditions for 14 days. Larger tumoroids were formed in the stemness-enhancing medium compared to smaller tumoroids seen in the serum-containing medium (Fig. 2 A-C). A highly significant difference in the tumoroid size between LuM1 and MMP3-null cells was observed under the stemness-enhancing culture conditions from day 3 until day 7 (Fig. 2 A-C). The size of MMP3-null tumoroids was significantly smaller compared to LuM1 tumoroids (Fig. 2 B, C).

Subsequently, we asked whether MMP3-KO and LuM1 cells were able to grow if they reseeded under the 2D culture conditions or not. We trypsinized tumoroids and reseeded under the 2D culture condition. Both cell types proliferated and reached confluency by day 7. More interestingly, LuM1 cells were able to grow into tumoroids even under the 2D culture condition, whereas MMP3-null cells were not (Fig. 2D).

These data suggest that the stemness-enhancing medium promotes the tumorigenic aggregation of tumor cells, whereas the serum-containing medium stimulates the cellular differentiation and decreasing the fusion of tumoroids. Besides, these findings indicate that loss of MMP3 has a great significance on inhibiting the tumoroid formation *in vitro*.

Preprints (www.preprints.org) | NOT PEER-REVIEWED | Posted: 25 March 2020 doi:10.20944/preprints202003.0371.v1

Peer-reviewed version available at Cancers 2020, 12, 1260; doi:10.3390/cancers12051260

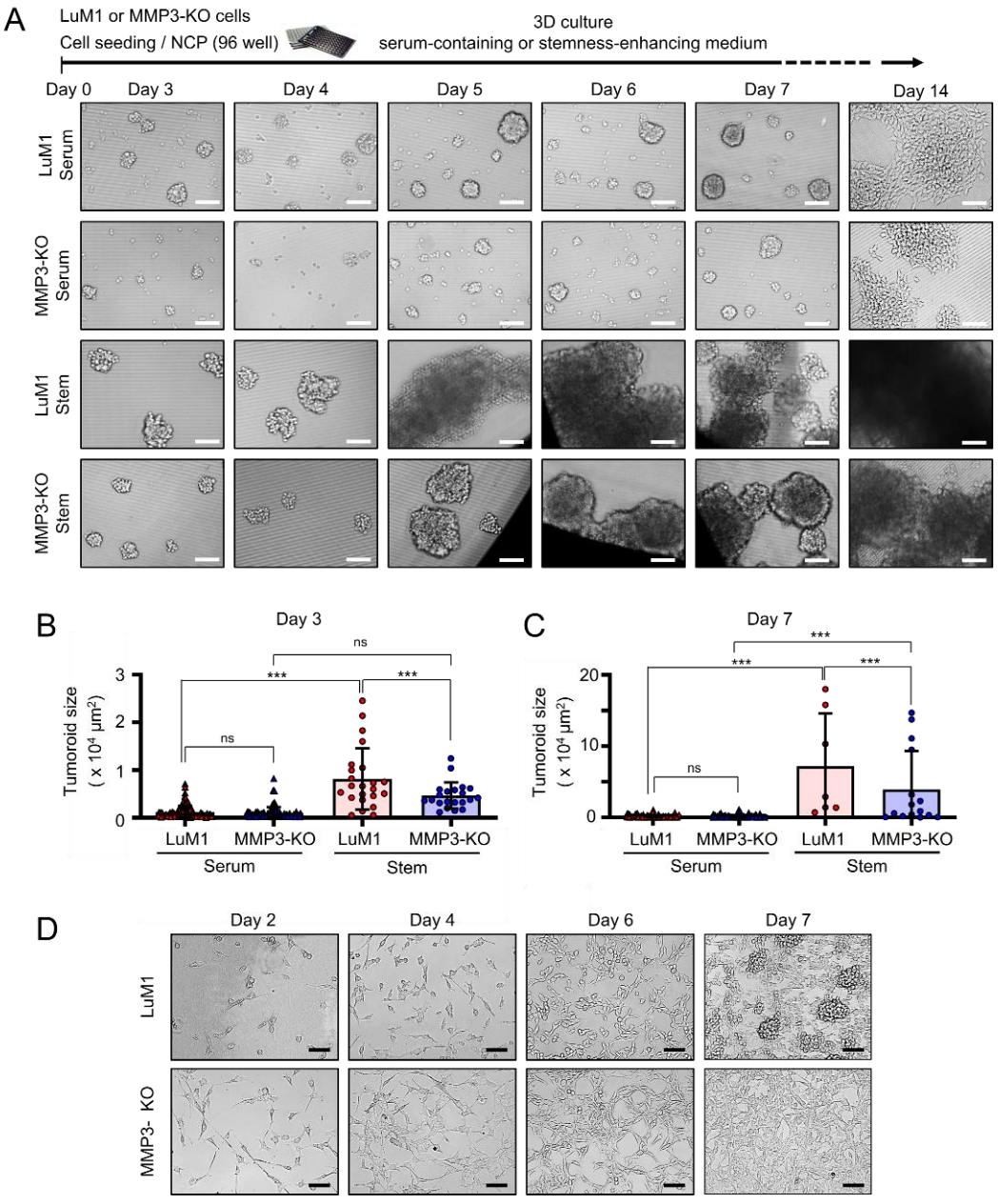

Figure 2: Loss of *Mmp3* reduces the *in vitro* tumorigenicity. (A-C) Tumoroids were formed in the NanoCulture Plate (NCP)-based 3D culture with a serum-containing or stemness-enhancing medium. **(A)** Representative images of the LuM1 and MMP3-KO tumoroids. The upper panel shows the experimental design. **(B, C)** Tumoroid size quantification on **(B)** day 3 and **(C)** day 7 of the tumoroid growth periods. Data were represented as Mean±SD, n=3, *P<0.05, **P<0.01, ***P<0.001; ns, not significant. **(D)** Representative images of re-cultured LuM1 and MMP3-KO cells in 2D culture. Tumoroids on day 14 were trypsinized and re-cultured under the 2D culture condition in serum-containing media. Scale bars, 100 µm. The experiments were repeated twice in Figure 1 A-D.

3.3. The addition of MMP3-rich EVs accelerated the in vitro tumorigenesis of MMP3-KO cells.

Preprints (www.preprints.org) | NOT PEER-REVIEWED | Posted: 25 March 2020 doi:10.20944/preprints202003.0371.v1

Peer-reviewed version available at Cancers 2020, 12, 1260; doi:10.3390/cancers12051260

We further investigated whether treating the MMP3-KO tumoroids with LuM1-EVs (MMP3-rich) or MMP3-KO-EVs (MMP3-null) would foster the *in vitro* tumorigenesis under the 3D culture system. Notably, the addition of LuM1-EVs resulted in a remarkable increase in the size of tumoroids and the formation of larger tumoroids, while the addition of MMP3-KO-EVs did not have any effect compared with the PBS-treated cells (Fig. 3A-C). A highly significant difference was observed in the size of tumoroids on day 3 and day 14 after the addition of LuM1-derived EVs compared to MMP3-KO-derived EVs or the PBS-treated group (Fig. 3B-D). In parallel, the comparison of the top 20 tumoroid sizes in the three groups revealed that the addition of LuM-1-derived EVs promoted the formation of enlarged tumoroids compared to the other two groups (Fig. 3D, E).

We thus found that that (i) MMP3-high, LuM1-derived EVs promoted the tumor growth *in vitro* and (ii) the loss of MMP3 in EVs diminished the protumorigenic properties of EVs.

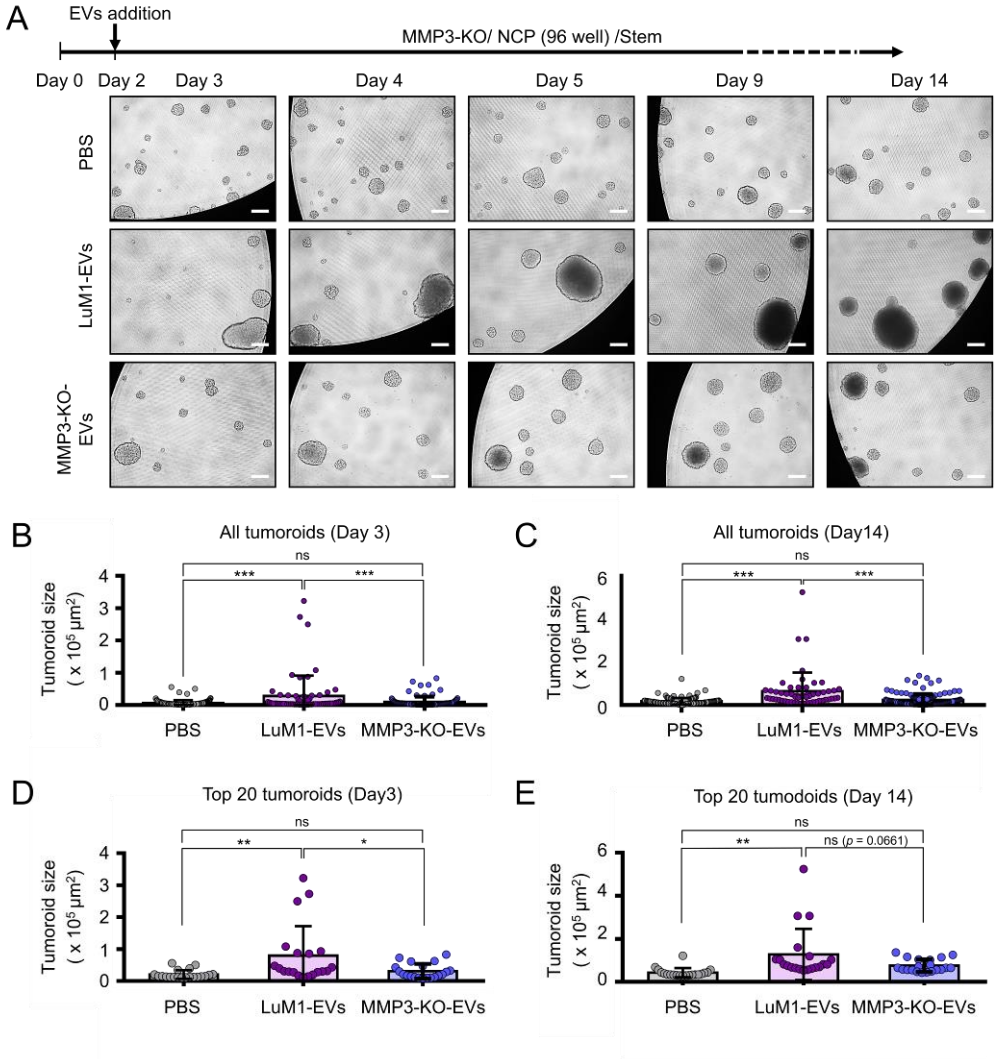

Figure 3: The addition of MMP3-rich EVs accelerated the *in vitro* tumorigenesis of MMP3-KO cells. MMP3-KO tumoroids were treated with PBS, LuM1-EVs, or MMP3-KO-EVs in the NCP-based 3D culture with the stemness-enhancing medium. **(A)** Experimental scheme (top) and representative photomicrographs of tumoroid maturation on the indicated timepoints. Scale bar, 100 µm. **(B, C)** Tumoroid size quantification on **(B)** day 3 and **(C)** day 14 of the tumoroid formation periods. Cell aggregates (>500 µm²) were considered to be tumoroids. (D, E) Top 20 tumoroids size quantification on **(D)** day 3 and **(E)** day

14. Data were represented as Mean±SD, n=3, *P<0.05, **P<0.01, ***P<0.001; ns, not significant. The experiments were repeated twice in Figure 2 A-E.

3.4. Establishment of fluorescent-labeled LuM1 and MMP3-null cells

It has been shown that EVs were derived from the plasma membrane [2] and could be labeled with palmitoylation signal-tagged fluorescent proteins [37]. To monitor the tumor EVs-uptake and exchange between cell populations, the plasma membrane of the LuM1 and MMP3-KO cells were labeled with palmitoylation signal-fused fluorescent reporters namely palmG and palmT, thereby green and red labeled cells were established (Fig. 4A, B).

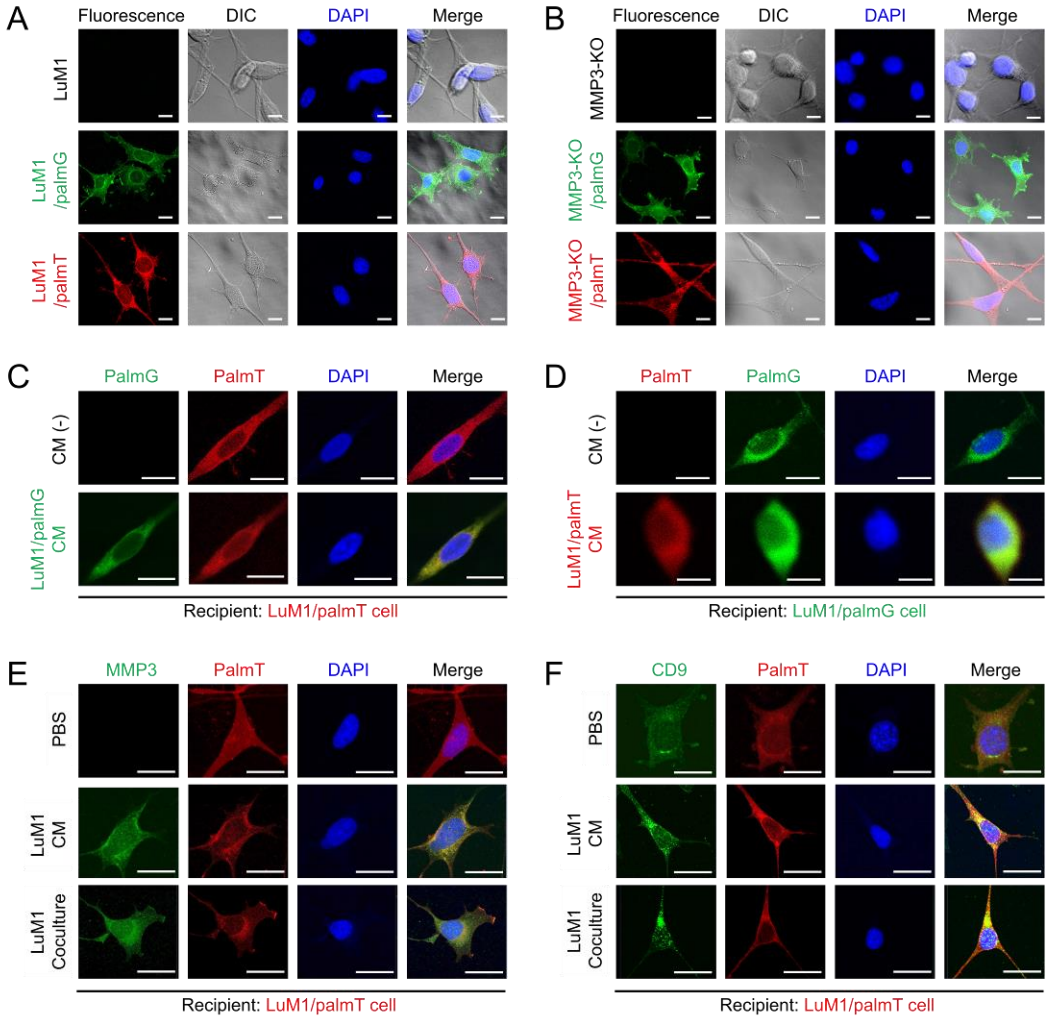

Figure 4: Establishment of fluorescent-labeled LuM1 and MMP3-KO cells. (A, B) Fluorescent labeled **(A)** LuM1 and **(B)** MMP3-KO cells. The stable cells were established by the transfection of expression constructs for palmT (red) and palmG (green) fluorescent proteins tagged with the palmitoylation signal. Images were taken using confocal laser scanning microscopy (CLSM). Non-fluorescent LuM1 and MMP3-KO cells were used as negative controls. **(C, D)** Molecular transfer of **(C)** palmG- and **(D)** palmT-labeled EVs from the conditioned medium (CM) of donor cells to recipient cells. **(C)** LuM1/palmT cells were treated with/without the CM of LuM1/palmG cells. **(D)** LuM1/palmG cells were treated with/without the CM of LuM1/palmT cells. **(E, F)** Immunostaining of **(E)** MMP3 and **(F)** CD9 in recipient MMP3-KO/palmT cells stimulated with

PBS, LuM1-CM, or coculturing with LuM1 cells in the Transwell system. DNA was stained with DAPI (blue). DIC, differential interference contrast. Scale bars, 20 μm. The experiments were repeated twice in Figure 4F.

Next, we confirmed the exchange of EVs between the cells. Two different colored fluorescent cells LuM1/palmG (green) and LuM1/palmT (red) cells were treated with each other conditioned media (CM) collected under the 2D culture condition. In this EVs exchange assay, if the red/green recipient cells took up the green/red-EVs from donor cells, an increase in the green/red fluorescence signals should be observed, whereas, in non-treated cells, no green/red fluorescence signals should be detected. Indeed, the green/red fluorescence was markedly detected in the cells treated with the CM of green/red cells, indicating that EVs were exchanged between the cells (Fig. 4C, D).

Additionally, we confirmed the EVs-mediated molecular transfer of MMP3 and CD9 under the 2D culture system by treating MMP3-KO cells with LuM1-CM or by co-culturing with the MMP3 producing LuM1 cells in the chamber well co-culturing system aka Transwell. Interestingly, MMP3 was restored and detected in the cytoplasmic and nuclear regions of MMP3-KO recipient cells after the addition of LuM1-CM or coculturing (Fig. 4E).

The CD9 expression level was low in the MMP3-KO cells as shown in Figure 1. However, CD9 was significantly increased in the nuclear and cytoplasmic regions of MMP3-KO recipient cells after the addition of LuM1-CM or coculturing (Fig. 4F). *Mmp3* was deleted at the genome level, while *Cd9* was not in the MMP3-KO cells. Therefore, as data interpretation, there were two possibilities including that (i) CD9 was transferred from LuM1-EVs to recipient cells and/or (ii) endogenous CD9 was induced in the recipient cells after the stimulation with LuM1-EVs.

Collectively, these data prove the successful labeling and exchanging of EVs between cell populations.

3.5. Penetration of tumor-derived MMP3 into organoids.

The bidirectional EVs-mediated transfer of cargo effectively influences the recipient phenotype to promote the development of an environment hospitable towards the cancer growth, invasion, and metastasis [43]. Moreover, the roles of EVs in the intercellular communication within the tumor microenvironment is increasingly acknowledged. We therefore examined whether MMP3 enriched in EVs and CM was transferred and penetrating MMP3-null recipient tumoroids by immunohistochemistry (IHC). MMP3 was well detected on the surface and inside of the recipient tumoroids after the addition of LuM1-EVs and LuM1-CM (Fig.5). Additionally, MMP3-null tumoroids contained more space between cells and thus more fragile, while the addition of MMP3-rich, LuM1-EV or –CM promoted the formation of solid tumoroids.

To examine the molecular transfer and penetration of MMP3 into tumoroids, we next stained the recipient tumoroids by immunofluorescence (IF). To eliminate non-specific reaction, we confirmed the specificity of the anti-MMP3 antibody in the LuM1/palmT tumoroids (Fig. S1).

To examine molecular penetration and tissue localization of MMP3, we next used CLSM. MMP3 from LuM1-EVs and –CM was found to penetrate the MMP3-null tumoroids (Fig. 6A). Notably, intracellular and intranuclear penetration of MMP3 in the recipient tumoroids was seen after the addition of MMP3-rich, LuM1-EVs (Fig. 6A, B). MMP3 transferred from EVs and CM were seen as speckles in cytoplasm and nuclei in the recipient MMP3-null tumoroids (Fig. 6B).

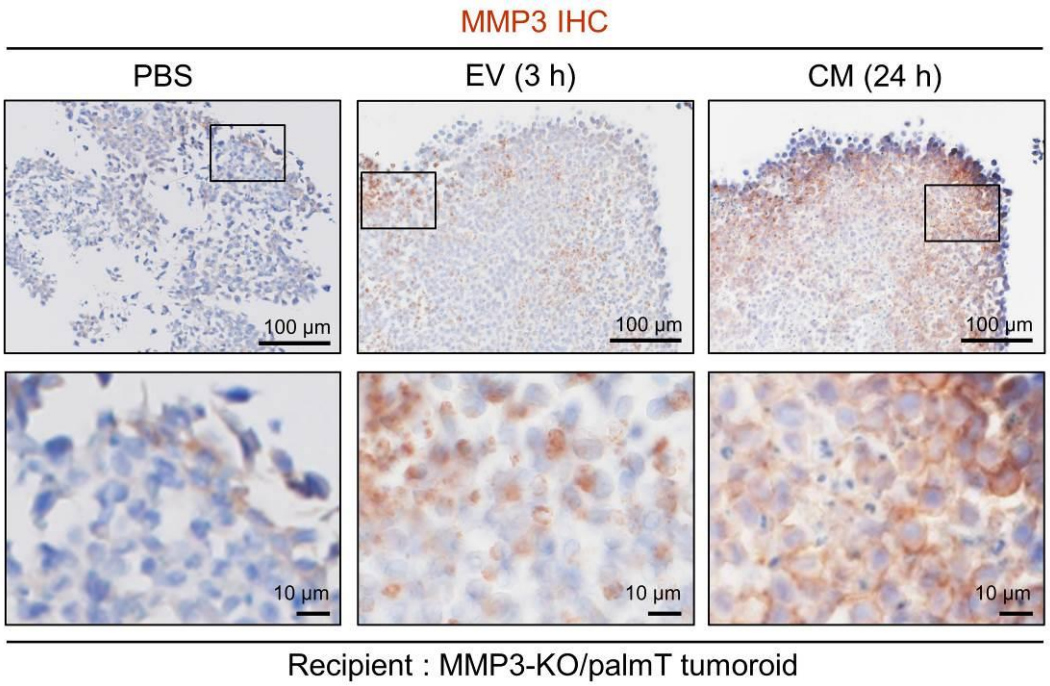

Figure 5. Molecular transfer and penetration of tumor-derived MMP3 into MMP3-null tumoroids. MMP3-KO/palmT tumoroids were treated with PBS, LuM1-EVs for 3hours, or LuM1-CM for 24 hours in the ULA-based 3D culture system. The tumoroids were fixed and tissue sections were prepared for IHC of MMP3. Brown, MMP3 IHC. Blue, counterstaining of nuclei. Scale bars; 100 μm (in low magnification images) and 10 μm (in high magnification images).

We have found that CD9 was decreased in MMP3-KO cells as shown in Fig. 1 and Fig. 4. We examined whether CD9 could be altered in the CD9-low, MMP3-KO recipient tumoroids by adding LuM1-EVs or -CM. CD9 was well stained in the recipient tumoroids, especially the parts close to the surface of tumoroids after the addition of the MMP3-rich CM or EVs (Fig. 7A). Moreover, CD9 and endogenous palmT in the recipient tumoroids became abundantly expressed on the cell surface and well co-localized seen as honeycomb shape, suggesting that CD9 contributed to cell-cell adhesion in the recipient tumoroids (Fig. 7B).

These findings indicate that These data suggested that LuM1-derived EVs and CM enhanced the solidity of MMP3-null tumoroids, which were relatively fragile. MMP3 was carried by LuM1-EVs, highly penetrative, and deeply transferred to the recipient MMP3-null tumoroids. Intranuclear transfer of MMP3 and the increase in CD9 could contribute to the increased solidity in the MMP3-KO tumoroids.

Preprints (www.preprints.org) | NOT PEER-REVIEWED | Posted: 25 March 2020 doi:10.20944/preprints202003.0371.v1

Peer-reviewed version available at Cancers 2020, 12, 1260; doi:10.3390/cancers12051260

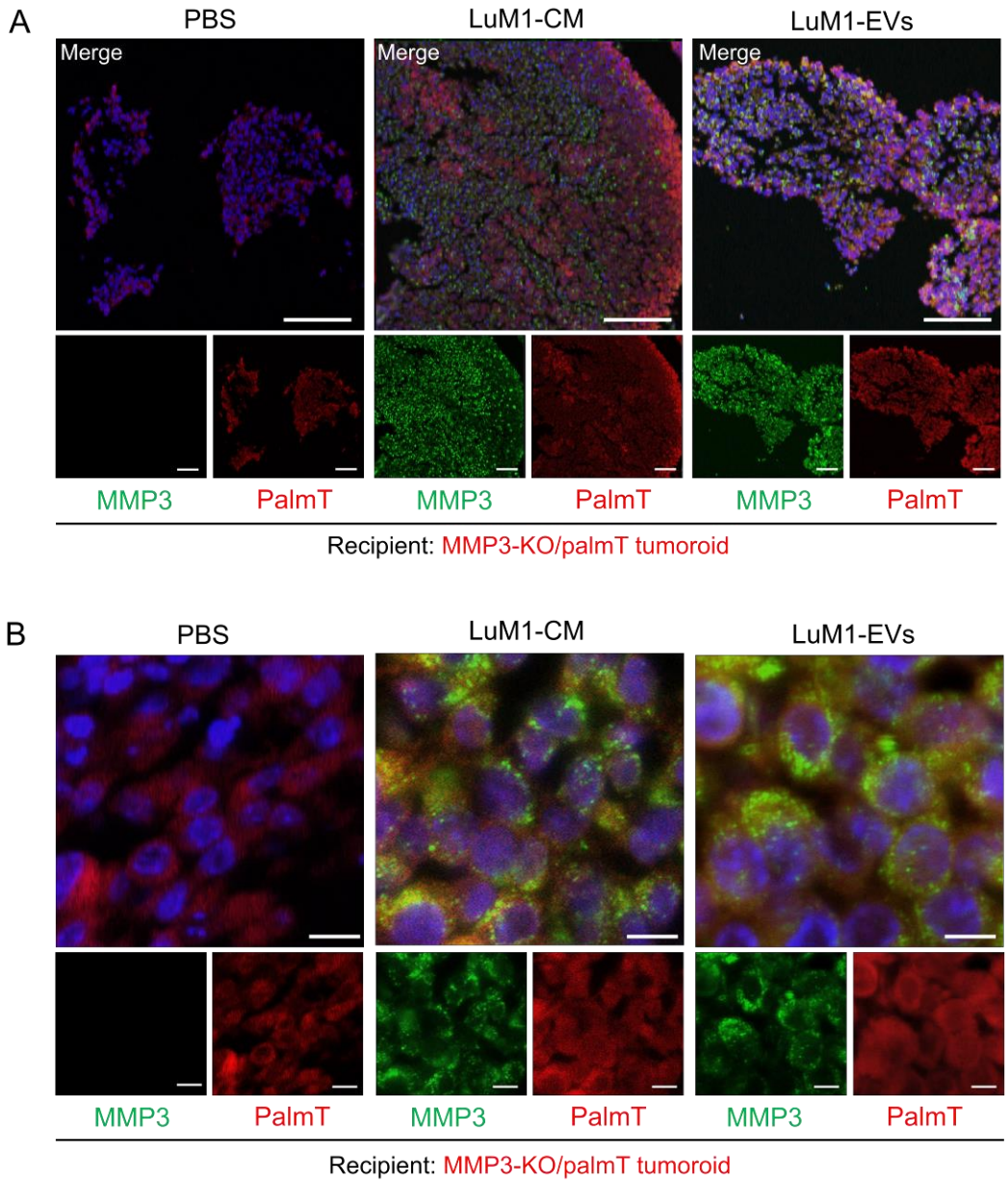

Figure 6: The EV-mediated deep transfer of MMP3 into tumoroids. MMP3-KO/palmT (red) tumoroids were treated with PBS, LuM1-CM, or LuM1-EVs for 24 hours in the ULA-based 3D culture system. MMP3 (green) was stained by immunofluorescence. Nuclei were stained blue with DAPI. Images were taken by CLSM. **(A)** low and **(B)** high magnifications were shown. Scale bars; 100 μm (in low magnification images) and 10 μm (in high magnification images).

Preprints (www.preprints.org) | NOT PEER-REVIEWED | Posted: 25 March 2020 doi:10.20944/preprints202003.0371.v1

Peer-reviewed version available at Cancers 2020, 12, 1260; doi:10.3390/cancers12051260

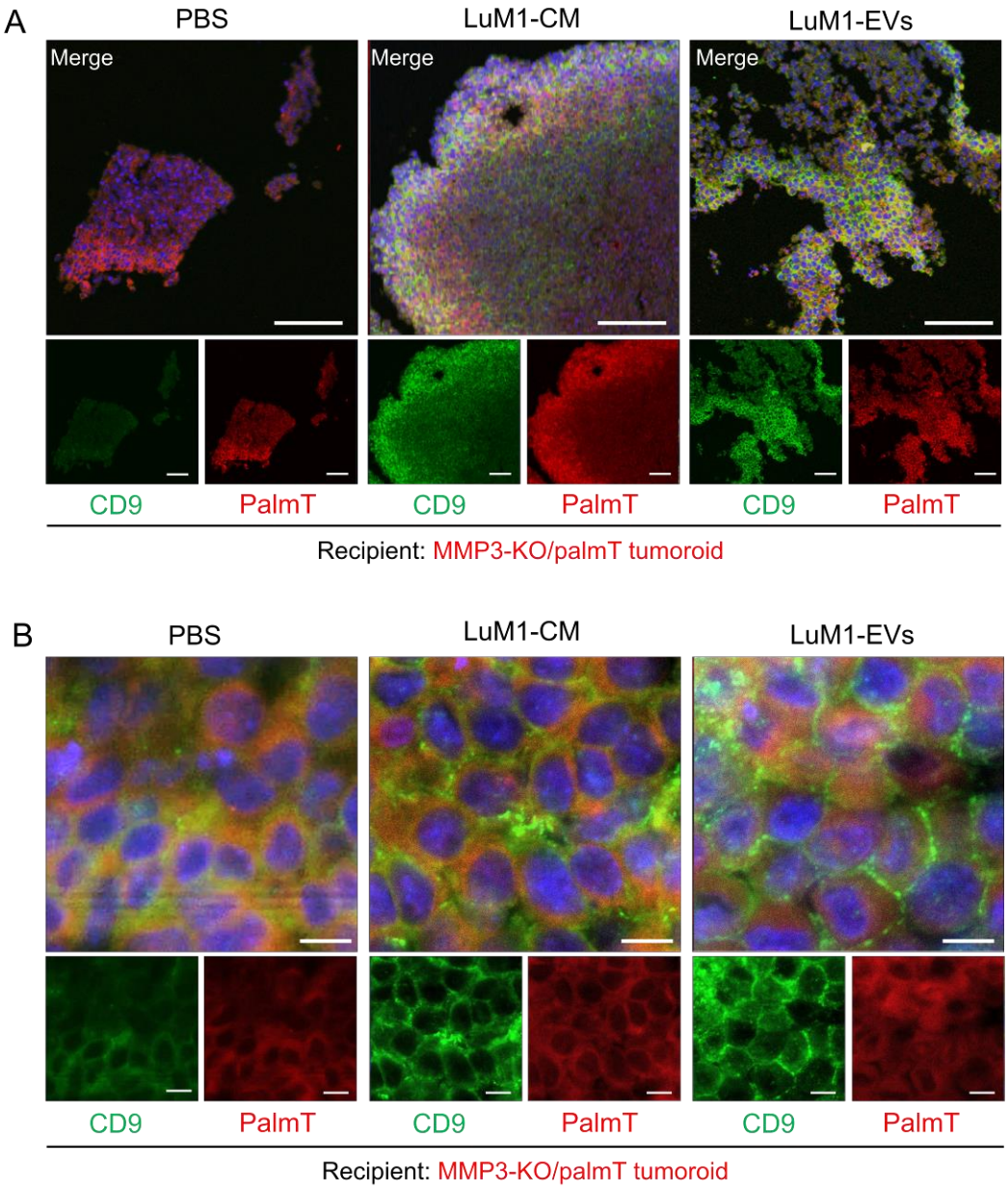

Figure 7: Treatment with LuM1-derived EVs and CM recovered CD9 in MMP3-null tumoroids. MMP3-KO/palmT (red) tumoroids were treated with PBS, LuM1-CM, or LuM1-EVs for 24 hours in the ULA-based 3D culture system. CD9 (green) was stained by immunofluorescence. Nuclei were stained blue with DAPI. Images were taken by CLSM. **(A)** low and **(B)** high magnifications were shown. Scale bars; 100 μm (in low magnification images) and 10 μm (in high magnification images).

3.8. Knockout of Mmp3 gene significantly decreased the transmissive potential of LuM1-EVs.

We have developed a method to examine the EV transfer to tumoroids by labeling EVs with red-fluorescent sphingolipids (Namba et al 2018 Front Oncol). In the present study, we monitored whether LuM1 tumoroid-derived or MMP3-KO tumoroid-derived heterogenous EVs (shown in Fig. 1) were differently transferred to the MMP3-null tumoroids over 24 hours. We found that the MMP3-null tumoroids rapidly internalized the MMP3-rich, LuM1-EVs at a highly significant rate compared to the

Preprints (www.preprints.org) | NOT PEER-REVIEWED | Posted: 25 March 2020 doi:10.20944/preprints202003.0371.v1

Peer-reviewed version available at Cancers 2020, 12, 1260; doi:10.3390/cancers12051260

MMP3-null EV from 4 hours to 24 hours post-EVs addition (Fig. 8A, B). Furthermore, the EVs uptake by tumoroids was increased in a time-dependent manner for 24 hours (Fig. 8B).

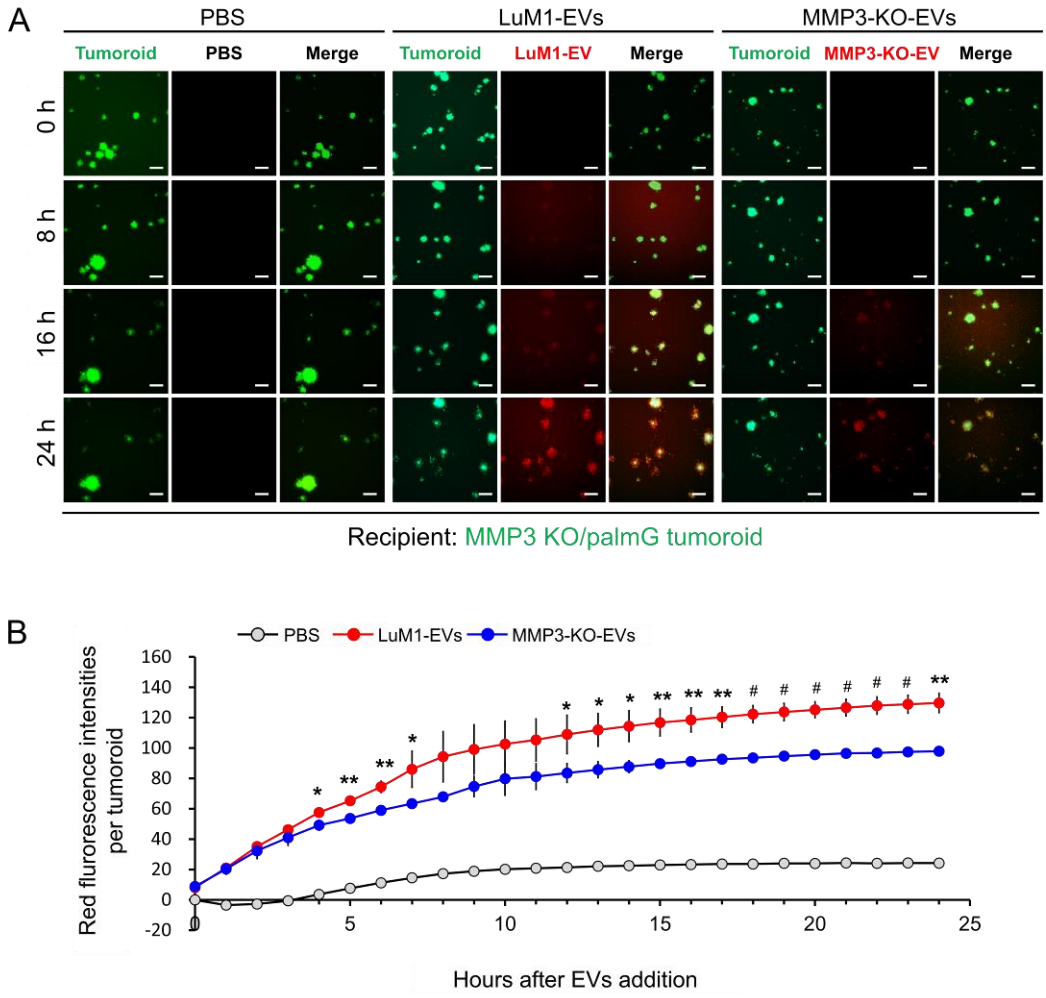

Figure 8: Knockout of MMP3 significantly decreased the transmissive potential of tumoroid-derived EVs. EVs were collected after 6 days from the culture supernatants of tumoroids that formed in ULA plates. EVs were fluorescently labeled with BODIPY TR Ceramide (red). The labeled EVs or PBS were added to the MMP3-KO/palmG (green) tumoroids at a concentration of 5 μg/1mL in the NCP-based 3D culture with the stemness-enhancing medium. The uptake of EVs was monitored over 24 hours using the high contents screening (HCS) system. **(A)** Time-course imaging of EV uptake (red) by MMP3-KO/palmG tumoroids (green) for 24 hours. Scale bar, 100 μm. **(B)** Red fluorescence intensities of transmitted EVs in MMP3-KO/palmG tumoroids. The average fluorescence intensity of the PBS treatment group at time point 0 h was evaluated as background and subtracted from raw values. Data were represented as Mean±SD, n=3, **P<0.05, **P<0.01, and #P<0.001 (LuM1-EVs versus MMP3-KO-EVs).

To sum up, these findings indicate that MMP3-rich, LuM1 tumoroid-derived EVs were highly transmissive and associated with tumoroids, while the loss of MMP3 in tumoroid-EVs reduced the transmissive and binding properties. These data also support our hypothesis that both endogenous and

Preprints (www.preprints.org) | NOT PEER-REVIEWED | Posted: 25 March 2020 doi:10.20944/preprints202003.0371.v1

Peer-reviewed version available at Cancers 2020, 12, 1260; doi:10.3390/cancers12051260

exogenous MMP3 play key roles in promoting the tumorigenesis, thereby MMP3-rich EVs were rapidly taken up by the MMP3-null tumoroids.

3.9. MMP3-enriched EVs and CM rescue the cell proliferation of MMP3-KO tumoroids.

In the course of our study, we compared the morphological characteristics of the LuM1 and MMP3-KO tumoroids by the histological (H&E) staining which revealed the development of central necrotic areas in the MMP3-KO tumoroid, but not in the LuM1 tumoroid (Fig. 9A). Additionally, there was a significant reduction in the Ki-67 expression, a marker of cell proliferation, in the MMP3-KO cells compared to their counterparts (Fig. 9B, C). Following the addition of MMP3-rich CM and EVs, the recipient MMP3-KO tumoroid displayed a highly proliferative phenotype as judged by the highly significant increase in Ki-67 expression index (Fig. 9B, C). These findings prove that MMP3 plays a crucial role in promoting cell proliferation in tumoroids and delaying the necrotic process.

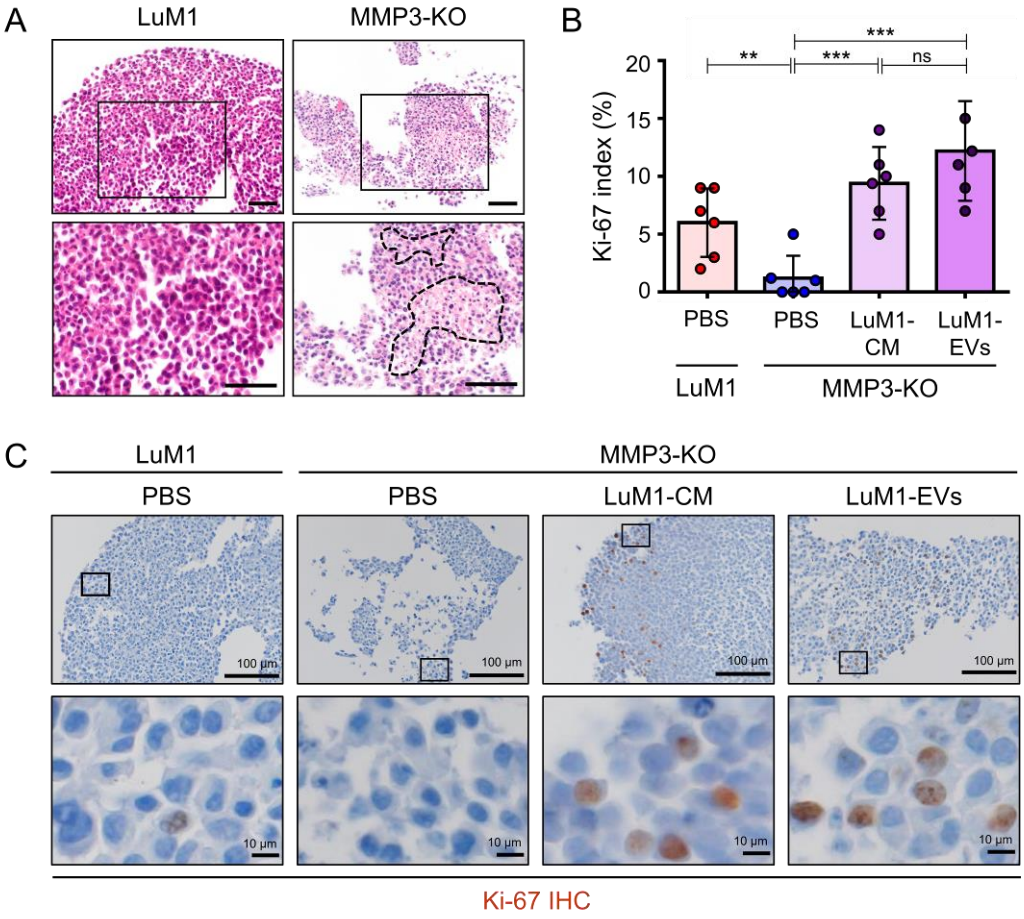

Figure 9: MMP3 enriched-EVs and CM rescue the proliferation of MMP3-KO tumoroids. (A) Hematoxylin and eosin (H&E) staining of the LuM1 and MMP3-KO tumoroids. Tumoroids were cultured in the ULA-based 3D culture system with stemness-enhancing medium for 8 days. Necrotic areas were enclosed with dotted lines. Scale bars, 50 μm. **(B, C)** LuM1 or MMP3-KO tumoroids were treated with PBS, LuM1-CM, or LuM1-EVs for 24 h and then Ki-67 was immunostained. **(B)** Ki-67 labeling index (%) and **(C)** Ki-67 immunostaining (brown) in the LuM1 and MMP3-KO tumoroids. Mean±SD, n=3, *P<0.05, **P<0.01, ***P<0.001; ns, not significant. Scale bars, 100 μm (in low magnification images) and 10 μm (in high magnification images). Experiments were repeated twice in Figure 9A.

4. Discussion

4.1. Summary

MMP3 is a proteolytic enzyme, as well as a transcriptional factor that plays a crucial role in tumor progression [20], [21], [24], [25], [44]. However, the roles of MMP3 within EVs had not unveiled before our study. We recently generated MMP3-KO cells by CRISPR/Cas9 system [20] and have analyzed their properties in EVs and tumorigenesis. In the current study, we found that MMP3 was abundantly detected in the high-metastatic cancer cells, their non-EV fluids, and EVs, although not in/from MMP3-KO cells. Thus, we newly explored (i) the oncogenic role of MMP3 on the *in vitro* tumoroid formation and on their EVs integrity under the 3D culture system, (ii) the tumorigenic potential of MMP3-rich versus MMP3-null EVs, and (iii) the EVs-mediated molecular transfer of MMP3 into the MMP3-KO tumoroids under the 3D culture system.

4.2. Potential mechanism of how MMP3 promotes tumorigenesis

It has been shown that the properties of 3D-tumoroids were more closely resemble the *in vivo* tumors compared to the 2D cultured cells thus this system has been effectively used for tumor study as well as drug screening assays [23], [25], [32]. Our current study investigated the effect of MMP3 loss on the *in vitro* tumoroid formation under the 3D culture system (Fig. 2). Indeed, the MMP3-null tumoroid size was significantly smaller than their parental counterpart. Of note, the MMP3-null tumoroids developed central necrotic areas; on the other hand, LuM1 tumoroids did not develop any cell death signs (Fig. 9A). More interestingly, only LuM1 were able to form cell aggregates when they were cultured under the 2D culture condition, but MMP3-KO cells were not (Fig. 2D). Therefore, it is conceivable that MMP3 could positively regulate tumoroid-forming factors through protein-protein interaction and/or transcriptional control. Several perspectives explained the functional role of MMP3 in the nucleus, for instance, nuclear MMP3 can act as a transcriptional cofactor, through binding and activating the promoter of connective tissue growth factor [CTGF aka cell communication network factor 2 (CCN2)] gene, which promotes chondrocyte growth, wound healing, and tumor progression [20], [45]. Moreover, intranuclear MMP3 can activate the transcription of some heat shock protein (HSP) family members such as Hsp70B and Hsp40 thereby, mediating resistance to apoptosis and anticancer drugs [46]. Our current data indicated that MMP3 might also regulate CD9 at transcriptional or post-transcriptional levels. Moreover, it has become clear that the function of MMPs was not only restricted to degrade or inactivate matrix proteins and that proteolysis by MMPs can modulate or even increase functions of substrate proteins [47]. For instance, the activities of many protein species were found to be positively regulated by MMP proteolysis including CCN2/CTGF [20], [48], [49], insulin growth factor binding proteins (IGFBPs) [50], heparin-binding epidermal growth factor (HB-EGF) [51], fibroblast growth factor receptor 1 (FGFR1) [52], interleukin-1beta (IL-1β) [53], and tumor necrosis factor-alpha (TNF-α) [54]. Such proteins activated by MMPs strengthen our *in vitro* findings that MMP3 can foster tumor development by modulating the activities of many signaling pathways and their receptors.

Our data also indicated that MMP3 is a regulator for the physical and biological characteristics of EVs. Tetraspanin CD9, a category-1 EV marker, was downregulated in MMP3-null cells and EVs compared to their counterparts, suggesting that MMP3-knockout reduced the endogenous production or stability and subsequent release of CD9-containing EVs. It has been known that tetraspanins, CD326/EpCAM (these are category-1 EV markers), and the tight junction protein claudin-7 partners associate with each other for cell-cell adhesion and apoptosis resistance [55]. Moreover, tetraspanin interaction with another tetraspanin and integrins often depended on palmitoylation [56], [57]. Therefore, MMP3-KO-triggered loss of CD9 could reduce cell-cell adhesion and EV-cell adhesion required for tumoroid integrity.

4.3. Release of L-EVs and s-EVs from 3D tumoroids

The morphological visualization of EVs showed abnormally disorganized shapes of EVs such as crescent moon-like and broken EVs associated with the *Mmp3* loss. These data indicated that MMP3 played key roles in maintaining structural proteins required for the integrity of EVs as well. Besides, we distinguished two subpopulations of 3D tumoroid-derived EVs, namely s-EVs (50-200 nm) and L-EVs (200-1000 nm) (Fig. 1 C-F). It is worth noting that under the 2D culture system both LuM1 and MMP3-KO cells secreted homogeneous intact s-EVs (50-300 nm diameter) [20]. This inconsistency is due to our current study was performed under the 3D culture system which is completely different from the 2D culture system. Thus, intra-tumoral hypoxia developed under the 3D culture model may be stimulated the production of L-EVs. The release of both s-EVs and L-EVs might be a key property of 3D tumoroids, a model resembling of tumors *in vivo*. It has been reported that adipocytes secreted L-EVs containing cytoskeletal proteins and molecular chaperones, whereas s-EVs were shown to contain ECM proteins [58]. Moreover, the proteomic analysis of s- and L-EVs derived from a colorectal cancer cell line revealed that s-EVs were enriched with proteins associated with cell-matrix adhesion and cell-cell junctions [59]. Similarly, s-EVs from fibrosarcoma cells showed similar enrichment for adhesion proteins [59]. Likewise, one of our recent studies has demonstrated that the prostate cancer (PC-3) cells release two types of vesicles, s-EVs (30-200 nm) under a non-heated condition, L-EVs (200-500 nm) and membrane-damaged EVs which were associated with HSP90α expression [8]. Notably, both membrane-damaged EVs and L-EVs were co-released upon the heat shock stress, suggesting that vesicular membranes were damaged by the stress [8]. Thus, the two different EVs populations may play distinct biological roles in recipient cells. We are currently challenging to separate the s- and L-EVs from the tumoroids and distinguish their properties.

4.4. Fluorescent labeling of EVs

Besides, we tagged the plasma membrane of LuM1/MMP3-null cells with palmitoylation sequence-fused fluorescent proteins, to enable the labeling of membrane vesicles that were released from the cells. Firstly, we developed fluorescent cells (Fig. 3), then we monitored the transmission and uptake of EVs. We detected a strong fluorescent signal of donor-derived EVs in recipient cells, indicating that the bidirectional exchange of EVs between the cells. PalmGFP and PalmtdTomato EV labeling strategy were designed to visualize and track multiple EV subtypes. By using these reporters, 0.22- and 0.8-μm sized EV populations, as well as sucrose density gradient with EV-marker proteins (such as Alix) were observed [37]. Using another EV tracking system, we tracked the uptake rate of MMP3-rich versus MMP3-null EVs for 24 hours. An increase in BODIPY TR ceramide/EVs signal was observed as early as 3 hours post-EVs exposure period, and the increase continued until it reached saturation at 24 hours (Fig. 8). Thus, both fluorescent-EV monitoring systems were useful for EV uptake assay. It has been shown that uptake of EVs occurred via multiple routes, such as the direct fusion between EVs and the plasma membrane [60], as well as EV internalization through lipid raft-, clathrin- and calveolae-dependent endocytosis, macropinocytosis and phagocytosis [61]–[66]. However, it is unclear which mechanism(s) is employed in different cell types under various conditions.

4.5. A potential mechanism of how MMP3-EVs promote tumor development.

Our study also demonstrated that MMP3 plays a pivotal role in different pathophysiological processes and tumor growth. We monitored the MMP3-null tumoroid growth following the addition of MMP3-rich and -null EVs. Interestingly, a remarkable increase in the tumoroid size of null cells was observed after receiving MMP3-rich EVs on day 1 and lasted until day 14. On the other hand, the addition of MMP3-null EVs did not have positive impacts on tumoroids formation, indicating the importance of exogenous MMP3 in the tumorigenesis (Fig. 8A, B). Several studies have reported that several MMP family members were

packaged in EVs from body fluids or various types of cell lines [20], [67]–[71]. Our current results are consistent with recent data that oncosomes enriched with MMP3 were highly transmissive and protumorigenic *in vitro* and *in vivo* [20]. MMP3-rich oncosomes were found to activate the CCN2/CTGF promoter and induce CCN2/CTGF, a matricellular protein essential for ECM integrity around cells, tumor-stromal interaction, and potentially for EVs integrity. McCready et al. reported that EVs released by the invasive breast cancer cell line, MDA-MB231, were enriched with HSP90α. Extracellular HSP90α was found to promote plasmin activation as well as increase cell invasion [72]. Another study indicated that HSP90α in the extracellular media of the MDA-MB-231 cell lines activated the extracellular proteases such as MMP2 and plasmin that initiate the degradation of ECM components and release of growth factors resulting in promoting tumor cell invasion [73]. These reports are consistent with our findings regarding the expression and roles of HSPs in tumor progression [8], [74], [75]. Therefore, tumor-derived EVs that are rich in MMP3 and HSPs are capable of modulating the ECM in a way, which fosters tumor progression.

Besides, EV-derived MMPs could promote proteolysis in recipient cells leading to tumor progression. Wang et al. have reported that EVs derived from adipocytes promoted lung cancer metastasis via transferring MMP3 that resulted in increasing the MMP9 activity in lung cancer cells [76]. It has been shown that one MMP can activate another MMP including other members of MMPs. Therefore, the high expression of active MMP3 and/or MMP9 could convert MMP family members into active forms. Indeed, we have shown that both MMP3 and MMP9 were expressed at high levels in LuM1 cells and essential for tumor progression [21]. Nevertheless, the loss of MMP3 was crucial to reduce tumor and EV development. These data indicate that exogenous MMP3 can be positioned at the higher-order in the protease cascade that promotes tumor progression in the recipient cells.

4.6. How extracellular MMP transfer into cell nuclei stimulates cell proliferation

We also confirmed the nuclear translation of MMP3 and CD9 mediated by EVs in parallel with the EVs-uptake under the 2D and 3D culture systems (Fig. 4-7). An elevation in the MMP3 and CD9 fluorescence signals was seen in the MMP3-null/CD9-low recipient cells, indicating that EVs can mediate molecular transfer of MMP3 and CD9. Moreover, we confirmed the cytoplasmic and nuclear localization of MMP3 and the cell surface, cytoplasmic, nuclear localization of CD9 after the EVs-exposure or CM addition (Fig. 4-7). Moreover, the Ki-67 expression, a marker of cell proliferation, was significantly increased in MMP3-KO tumoroids after 24 hours from the addition of MMP3-rich CM/EVs (Fig. 9B, C). The mechanism of how extracellular MMP3 was transmitted into cell nuclei leading to cell proliferation was not completed in the present study but discussed below. Several perspectives explained the functional role of MMP3 in the nucleus, for instance, our research group has reported that nuclear MMP3 can act as a transcriptional factor, through binding and activating the promoter of *CCN2/CTGF* gene, which promoted chondrocyte growth, wound healing, and tumor progression [14], [20], [44], [77], [78]. Moreover, we reported that nuclear MMP3 activated the transcription of some HSP family members such as Hsp70B and Hsp40 thereby, mediating resistance to apoptosis [46]. Additionally, we reported that MMP3 was localized in the nucleus where this protein promoted the proliferation, migration, and metastasis of aggressive adenocarcinoma cells [21]. Therefore, it is conceivable that EV-derived, as well as non-vesicular MMP3, are transmissive into cells intranuclearly where MMP3 can activate *CCN2/CTGF*, *HSPs*, and other genes that can stimulate cell proliferation.

5. Conclusion

Our study demonstrated that the loss-of-function of MMP3 significantly decreased the 3D-tumoroids formation *in vitro*, reduced in the tetraspanin CD9 levels and, resulted in destabilizing the EVs structural integrity. Moreover, we proved the successful labeling, exchanging of EVs between cells, and established a bidirectional EV transfer assay system. We confirmed the EVs-mediated molecular transfer of MMP3 into

the MMP3-KO tumoroids under the 3D culture system. Also, we found that the addition of MMP3-enriched oncosomes fostered the tumorigenicity and increased the proliferation of MMP3-null cells. Thus MMP3-enriched oncosomes are highly transmissive and protumorigenic.

6. Materials and methods

6.1. Cells

A rapidly metastatic murine cancer cell line LuM1 [23], [25], [79] and MMP3-KO cells line [20] were maintained in RPMI-1640 with 10% fetal bovine serum (FBS) and penicillin, streptomycin, and amphotericin B. MMP3-KO cells were established using the CRISPR/Cas9 system from the LuM1 cell line [20]. Briefly, Cas9 protein and guide RNA that targets *Mmp3* exon 1 were co-transfected into LuM1 and stable MMP3-KO clones with frame-shifting deletion were obtained [20].

6.2. Tumoroid culture

Tumoroids were formed in the 3D culture systems using NanoCulture Plate (NCP) (Medical & Biological Laboratories, Nagoya, Japan) or ultra-low attachment (ULA) culture plates/dishes (Greiner, Kremsmunster, Austria) within mTeSR1 stem-cell medium (Stemcell Technologies, Vancouver, Canada) or the above-mentioned serum-containing medium as described previously [19], [23]–[25] .

For quantification of tumoroids size and number, cells were seeded in a 96 well NCP for 14 days at a concentration of 5.0 x 10^3 cells in 200 μL mTeSR1 or RPMI-1640 media with 10% FBS. Tumoroid maturation was monitored every day and photographed using the Floid cell imaging station (Thermo Fisher, Waltham, MA, USA) from day 1 until day 7 and a BZ-X microscope (Keyence, Osaka, Japan) starting from day 10 until the end of the experiment day 14. The tumoroid size was measured using Image J software (NIH, Bethesda, MD, USA).

6.3. 2D re-seeding assay

Tumoroids were cultured in the 3D and stem-cell medium condition for 14 days and detached by trypsin/EDTA. The detached cells were re-seeded in a 24-well 2D culture plate at a concentration of 1.5 × 10^4 cells per well in RPMI-1640 with 10% FBS. The cell images were taken by using the Floid cell imaging station (Thermo Fisher, Waltham, MA, USA) on day 2, 4, 6, and 7 after the seeding.

6.4. Preparation of EVs and conditioned media

Tumoroid-derived EVs and CM were used for tumoroid formation assays. Otherwise, 2D cultured cells-derived CM was used for 2D experiments. EVs were prepared from culture supernatants of tumoroids using a modified polymer-based precipitation method (Eguchi et al., 2020; Fujiwara et al., 2018; Ono et al., 2018). Briefly, cells were seeded on a 10-cm ULA dish at a density of 1.0 × 10^6 cells per 8 mL mTeSR1 medium and cultured for 6 days. The formed tumoroids were washed with PBS (-), and then further cultured in serum-free medium (4 mL per dish) for 2 days. Cell culture supernatant was collected and centrifuged at 2,000 × *g* for 30 min at 4°C to remove detached cells. The supernatant was then centrifuged at 10,000 × *g* for 30 min at 4°C to remove cell debris. The supernatant (8 mL) was concentrated to less than 1 mL by using an Amicon Ultra-15 Centrifugal Filter Devices for M.W. 100k (Merck Millipore, Burlington, MA). The concentrate was applied to the Total EVs Isolation System (Thermo Fisher, Waltham, MA, USA). The pass-through was concentrated using an ultrafiltration device for molecular weight 10 kD and used as a non-EV fraction. The EV fraction was suspended in 100 μL PBS (-) and used 3D-tumoroid-EVs. Protein concentration was measured using a micro BCA protein assay kit (Thermo Fisher, Waltham, MA, USA).

Peer-reviewed version available at Cancers 2020, 12, 1260; doi:10.3390/cancers12051260

For the 3D tumoroid culture system, CM wase collected from donor tumoroids on 6 days from culturing in mTeSR1 medium.

For immunofluorescence in the 2D culture system, culture supernatants were collected from serum-free media of 2D-cultured donor cells during the exponential growth phase (70% confluence). The culture supernatants were centrifuged at 2,000 x *g* for 15 min to get rid of cells and debris, followed by diluting in a ratio 1:1 with a fresh culture medium. The CM was stored at -80°C. Recipient cells were treated with the CM for 48 hours.

6.5. Transmission electron microscopy

As described previously [8], [19], a 400-mesh copper grid coated with formvar/carbon films was hydrophilically treated. The EVs suspension (5-10 μL) was placed on Parafilm, and the grid was visualized at 5,000, 10,000, or 20,000 times magnification with an H-7650 transmission electron microscope (TEM) (Hitachi, Tokyo, Japan) at the Central Research Laboratory, Okayama University Medical School.

6.6. Particle diameter distribution

As described previously [8], [11], 40 μL of EV fraction within PBS (-) was used. Particle diameters of the EV fractions in a range between 0 and 6,000 nano-diameters were analyzed in Zetasizer nano ZSP (Malvern Panalytical, Malvern, UK).

6.7. Western blotting

Western blotting was performed as described [8], [74]. Cells were cultured for 6 days on a 6 well ULA plate at a density of 3.0×10^5 cells per 3 mL mTeSR1 medium in a well. Cells were further cultured in serum-free media for 2 days. On day 8, the supernatants and tumoroids were collected, centrifuged at 2000 x *g*, 4°C for 5 min. The supernatants were used for EV preparations as mentioned above. To prepare whole cell lysate (WCL), tumoroids were lysed in a RIPA buffer (1% NP-40, 0.1% SDS, and 0.5% deoxycholate, and EDTA-free protease inhibitor cocktail in PBS) using 25-gauge syringes. The cell lysate was incubated for 30 min on ice and then centrifuged at 12,000 *g* for 20 min at 4°C. The preparation method of EV and non-EV fraction was described above. The supernatant was used as WCL. The same protein amounts for each lane were subjected to sodium dodecyl sulfate-polyacrylamide gel electrophoresis (SDS-PAGE), followed by transfer to a polyvinylidene fluoride (PVDF) membrane using a semi-dry transfer system. The membranes were blocked in 5% skim milk in Tris-buffered saline containing 0.05% Tween 20 for 60 min at room temperature (RT) and then incubated overnight with rabbit monoclonal antibodies; anti-MMP3 (EP1186Y, ab52915, Abcam, Cambridge, UK) or anti-CD9 (EPR2949, ab92726, Abcam, Cambridge, UK). The membranes were incubated with horseradish peroxidase (HRP)-conjugated secondary antibodies. For GAPDH, the HRP-conjugated anti-GAPDH mouse monoclonal antibody (HRP-60004, Proteintech, Rosemont, IL, USA) was used. Blots were visualized with the ECL substrate (Merck Millipore, Burlington, MA, USA).

6.8. Coomassie blue staining

Protein samples (1 μg each) were loaded on the SDS-PAGE. After the electrophoresis run, the gel was stained with Coomassie Brilliant Blue R-250 solution (1610436, Bio-Rad) for 30 min with gentle agitation followed by washing with the destaining solution (50% methanol, 10% glacial acetic acid) for 2 hours until the background became less dark.

6.9. EV-driven in vitro tumorigenesis

MMP3-KO cells were seeded at 5.0 x 10^3 cells per 200 µL mTeSR1 medium in a well of 96-well NCP. After two days, EVs derived from 3D-tumoroids (LuM1 or MMP3-KO) were added to MMP3-null tumoroids at a final concentration of 5 µg per 1 mL. Then the plate was centrifuged at 1,800 × *g* for 1 hour at 4°C to increase the internalization of EVs into the tumoroids (Lai et al., 2015).

The MMP3-KO tumoroids maturation was monitored over 14 days using a microscope FSX100 (Olympus Life Science, Tokyo, Japan). Then tumoroid size was measured using Image J.

6.10. Palm fluorescent cells

The lentiviral reporter constructs of CSCW-palmitoylation signal-tandem dimer Tomato (palmT) and CSCW-palmitoylation signal-EGFP (palmG) were kindly gifted from Dr. Charles P. Lai [37]. For virus production, HEK293T cells at 70-80% confluence were transfected with PalmT or PalmG constructs, psPAX2 packaging plasmid, and pMD2.G envelope plasmid using PEI max (Polysciences). LuM1 or MMP3-KO cells were infected by using the spinfection method with the viral solution. Infected/transduced stable cells were selected using puromycin. Isolation of single clones was carried out by limiting dilution method. We established palmtdTomato-expressed LuM1 cells (designated LuM1/palmT), palmGFP-expressed LuM1 cells (designated LuM1/palmG), palmGFP-expressed MMP3-KO cells (designated MMP3-KO/palmT), and palmGFP-expressed MMP3-KO cells (designated MMP3-KO/palmG). To confirm fluorescent labeling, the palm fluorescent cells were seeded on a type I collagen-coated coverslip in a 24-well plate at a density of 1 × 10^4 cells per well in a serum-containing culture media and cultured for 48 hours.

6.11. EVs exchange assay

Two different colored fluorescent cells (LuM1/palmG and LuM1/palmT cells) were used as donor cells or recipient cells with each other in the 2D culture system. The donor cells were seeded at 1 × 10^6 cells in a 60 cm dish and cultured overnight in a serum-containing culture media. The grown cells of 70-80% confluence were washed twice with PBS, then the culture media was replaced with serum-free medium and cultured for further 2 days. The culture supernatant was collected and centrifuged at 2,000 × *g* for 15 min at 4°C to remove detached cells and the supernatants were diluted in a ratio 1:1 with a fresh culture medium and used as CM. Recipient cells were seeded on a type I collagen-coated coverslip inserted in a 24-well plate at a density of 1 × 10^4 cells per well and cultured for 24 hours in a serum-containing culture media. The recipient cells were treated by donor cells-derived CM for 48 hours.

For coculturing, recipient MMP3-KO cells were seeded on coverslips. LuM1-donor cells (1 × 10^4 cells per well) were seeded on a culture insert with 0.45-µm pore (Greiner, Kremsmunster, Austria) in a 24 well plate. The insert with donor cells was placed on the well containing the recipient cells and cocultured for 48 hours.

6.12. 2D confocal laser-scanning microscopy

Cells were fixed in 4% paraformaldehyde (PFA) for 10 min at RT and permeabilized with 0.5% Tween-20 for 10 min. For blocking the non-specific reaction of primary antibodies, cells were blocked in 10% normal goat serum solution (Dako, Tokyo, Japan) for 30 min, then incubated overnight at 4℃ with rabbit anti-MMP3 antibody (EP1186Y, ab52915, Abcam, Cambridge, UK) or rabbit anti-CD9 antibody (EPR2949, ab92726, Abcam, Cambridge, UK), for overnight at 4°C and subsequently with a secondary antibody, goat anti-rabbit IgG Alexa Fluor 488 (A-11034, Thermo Fisher, Waltham, MA, USA) for 1 hour at RT. As a negative control, the same protocol was performed without primary antibody staining. Washes after antibody reactions were done with PBS, three times for 3 min each, on a shaker at RT. The mounting and DNA staining was performed by using Immunoselect Antifading Mounting Medium DAPI (SCR-038448,

Dianova, Germany). Fluorescent images were taken using a confocal laser scanning microscopy LSM780 (Carl Zeiss, Oberkochen, Germany) at Central Research Laboratory, Okayama University Medical School.

6.13. Immunohistochemistry of tumoroids

For tumoroid formation, cells were cultured for 6 days at a density of 3.0 x 10^5 per 3 mL mTeSR1 in a well of a 6-well ULA plate. Then tumoroids were treated with PBS, the 3D-tumoroid LuM1-EVs at a final concentration of 5 μg/mL or the 3D-tumoroid LuM1-CM (diluted 1:1 with fresh mTeSR1) for 24 hours. Then the plate was centrifuged at 1,800 × *g* for 1 hour at 4°C to increase the internalization of EVs into the tumoroids (Lai et al., 2015). Tumoroids were washed with PBS and fixed in 4% PFA for 10 min. Tumoroids were additionally washed with PBS for 5 min 3 times and embedded in paraffin. Tumoroids sections (5 μm thickness) were deparaffinized and hydrated through xylenes and graded alcohol series. Antigen retrieval was performed by heating the specimens in Tris/EDTA buffer, pH 9.0 (Dako target retrieval solution S2367, DAKO, Carpenteria, CA) using a microwave for 3 min for CD9 IHC or by autoclaving in 0.01M citrate buffer pH 6.0 (sodium citrate dihydrate, citric acid; Sigma Aldrich, USA) in a pressure cooker for 8 min for IHC of MMP3 and Ki-67. Sections were treated with blocking solution (Dako) for 30 min at RT, then incubated with primary antibodies; rabbit anti-CD9 (EPR2949, ab92726, Abcam, Cambridge, UK), rabbit anti-MMP3 (EP1186Y, ab52915, Abcam, Cambridge, UK), or rat anti-Ki-67 antibody (TEC-3, M7249, Dako); individually at 4°C overnight.

For 3D immunofluorescence and CLSM of MMP3 and CD9, sections were subsequently with a secondary antibody goat anti-rabbit IgG, Alexa Fluor 488 (A-11034, Thermo Fisher, Waltham, MA, USA) for 1 hour at RT. Then samples were counterstained with 1 mg/mL of DAPI (Dojindo Laboratories, Kumamoto, Japan). Fluorescent images were taken using a confocal laser scanning microscopy LSM780 (Carl Zeiss, Oberkochen, Germany) at Central Research Laboratory, Okayama University Medical School.

For IHC staining of Ki67 and MMP3, a biotinylated secondary antibody was applied for 30 min (Vector Lab, Burlingame, CA) and the color was developed with 3, 3'-diaminobenzidine (DAB) (Histofine DAB substrate; Nichirei, Tokyo, Japan). Then, samples were counterstained with Myer's hematoxylin and images were taken using an optical microscope BX53 (Olympus). To calculate the Ki-67 labeling index (%), we counted approximately 100 Ki67-positive cells were counted in random five fields under the 40× objective. Areas with severe inflammation and necrosis were avoided. The Ki-67 labeling index (%) was calculated by dividing the total Ki-67 positive cells by the total numbers of cells multiplied by 100.

6.14. Hematoxylin and eosin staining

For tumoroid formation, LuM1 or MMP3-KO cells were cultured for 8 days on 6 well ULA plates at a density of 3.0 x 10^5 per 3mL mTeSR1 per well. Then tumoroids were washed with PBS, fixed in 4% PFA for 10 min, and embedded in paraffin. Tumoroids sections (5 μm thickness) were deparaffinized in a series of xylene for 15 min, rehydrated in graded ethanol solutions and washed well in distilled water. Then sections were incubated in Harris hematoxylin solution for 10 min and rinsed in tap water until the water was colorless. Finally, after sequential treatment with hydrogen chloride and 80% ethanol solution, sections were incubated in eosin for 7 min.

6.15. Tracing EV-uptake in vitro

Ten micrograms of tumoroid-derived EVs were incubated with 0.25 μM BODIPY TR Ceramide (Thermo Fisher, Waltham, MA, USA) for 20 min at 37°C. Excessive BODIPY TR Ceramide was removed with Exosome Spin Columns (MW 3000) (Thermo Fisher, Waltham, MA, USA). Cells were seeded at a concentration of 5.0 x 10^3 cells per 200 μL mTeSR1 in a well of 96-well NCP. The next day, EVs were added at a final concentration of 5 μg/mL. The EVs-uptake was monitored over 24 hours using the

ArrayScan High Content Screening (HCS) system (Thermo Fisher, Waltham, MA, USA). The fluorescence intensity of each cell was determined using a filter set (485/594) for (GFP/ BODIPY TR). The average fluorescence intensity of the PBS treatment group at time point 0 hours was evaluated as background and subtracted from raw values.

6.16. Statistical analysis

Statistical significance was calculated using GraphPad Prism and Microsoft Excel. The difference between the sets of data was analyzed using ANOVA Tukey's multiple comparisons test and all data are expressed as the mean ± standard deviation unless otherwise indicated.

Acknowledgments: We thank Haruo Urata for TEM operation, Kazuko Kobayashi for Zetasizer operation, Eriko Aoyama and Masaharu Takigawa for ArrayScan operation.

Conflicts of interest: The authors have no competing financial interests to declare.

Funding: This work was funded by JSPS KAKENHI, grant numbers JP17K17895 (YO), JP17K11642 (TE), JP17K11669 (TE, CS), 17K11643 (CS, TE), JP18K09789-KN (TE), 19H04051-HO (HO, TE), 19H03817-MT (MT, TE), Suzuken Memorial Foundation (TE), and by Ryobi Teien Memorial Foundation (CS, KO, TE). E.A.T. was supported by the Egypt-Japan Education Partnership (EJEP) grant.

Author Contributions: E.A.T. carried out most of experimentations, formal analysis, and wrote the manuscript under supervision by T.E. and C.S. T.E. conceived, conceptualized and managed the study, interpreted, made use of, and visualized data, and edited the manuscript. Y.O. established MMP3-null cells using CRISPR-Cas9. C.S. designed experimental protocols and visualized data. H.K., M.W.O., H.N. and E.A.T. performed immunohistochemistry. E.A.T., A.E.S., and S.K. amplified and purified plasmids. Y.L. validated and visualized data. A.S., K.O., C.S., and T.E. acquired funding and mentored. All authors reviewed the manuscript.

Supplementary items: Figure S.1. The specificity of the MMP3 antibody. (A) Positive (B) and negative controls; LuM1/palmT tumoroids were stained with or without the MMP3 antibody, then stained with the secondary AF488 antibody. w/o Ab; without antibody. Scale bar 100 μm.

References

[1] M. Yanez-Mo *et al.*, "Biological properties of extracellular vesicles and their physiological functions.," *J. Extracell. vesicles*, vol. 4, no. 2015, p. 27066, 2015.

[2] G. G. G. Raposo and W. Stoorvogel, "Extracellular vesicles: Exosomes, microvesicles, and friends," *J. Cell Biol.*, vol. 200, no. 4, pp. 373–383, Feb. 2013.

[3] M. Colombo, G. Raposo, and C. Théry, "Biogenesis, Secretion, and Intercellular Interactions of Exosomes and Other Extracellular Vesicles," *Annu. Rev. Cell Dev. Biol.*, vol. 30, no. 1, pp. 255–289, Oct. 2014.

[4] Y. Fujita, Y. Yoshioka, and T. Ochiya, "Extracellular vesicle transfer of cancer pathogenic components," *Cancer Science*, vol. 107, no. 4. Blackwell Publishing Ltd, pp. 385–390, 01-Apr-2016.

[5] M. M. Durcin *et al.*, "No Title," *J. Extracell. vesicles*, vol. 6, no. 1, p. 1305677, Apr. 2017.

[6] C. Tucher *et al.*, "Extracellular vesicle subtypes released from activated or apoptotic T-lymphocytes carry a specific and stimulus-dependent protein cargo," *Front. Immunol.*, vol. 9, no. MAR, Mar. 2018.

[7] T. Vagner *et al.*, "Large extracellular vesicles carry most of the tumour DNA circulating in prostate cancer patient plasma," *J. Extracell. Vesicles*, vol. 7, no. 1, p. 1505403, Jan. 2018.

[8] T. Eguchi *et al.*, "Cell Stress Induced Stressome Release Including Damaged Membrane Vesicles and Extracellular HSP90 by Prostate Cancer Cells," *Cells*, vol. 9, no. 3, p. 755, Mar. 2020.

[9] M. C. Patton, H. Zubair, M. A. Khan, S. Singh, and A. P. Singh, "Hypoxia alters the release and size

distribution of extracellular vesicles in pancreatic cancer cells to support their adaptive survival," *J. Cell. Biochem.*, vol. 121, no. 1, pp. 828–839, Jan. 2020.

[10] C. Théry *et al.*, "Minimal information for studies of extracellular vesicles 2018 (MISEV2018): a position statement of the International Society for Extracellular Vesicles and update of the MISEV2014 guidelines," *J. Extracell. Vesicles*, vol. 7, no. 1, Jan. 2018.

[11] T. Fujiwara *et al.*, "Carcinogenic epithelial-mesenchymal transition initiated by oral cancer exosomes is inhibited by anti-EGFR antibody cetuximab," *Oral Oncol.*, vol. 86, no. July, pp. 251–257, 2018.

[12] E. A. Taha, K. Ono, and T. Eguchi, "Roles of extracellular HSPs as biomarkers in immune surveillance and immune evasion," *Int. J. Mol. Sci.*, vol. 20, no. 18, Sep. 2019.

[13] G. Berg, M. Barchuk, and V. Miksztowicz, "Behavior of Metalloproteinases in Adipose Tissue, Liver and Arterial Wall: An Update of Extracellular Matrix Remodeling," *Cells*, vol. 8, no. 2, p. 158, Feb. 2019.

[14] R. Visse and H. Nagase, "Matrix metalloproteinases and tissue inhibitors of metalloproteinases: Structure, function, and biochemistry," *Circulation Research*, vol. 92, no. 8. pp. 827–839, 02-May-2003.

[15] H. Nagase, R. Visse, and G. Murphy, "Structure and function of matrix metalloproteinases and TIMPs," *Cardiovascular Research*, vol. 69, no. 3. Oxford Academic, pp. 562–573, 15-Feb-2006.

[16] E. S. Radisky and D. C. Radisky, "Matrix metalloproteinases as breast cancer drivers and therapeutic targets," *Front. Biosci. - Landmark*, vol. 20, no. 7, pp. 1144–1163, 2015.

[17] C. Tallant, A. Marrero, and F. X. Gomis-Rüth, "Matrix metalloproteinases: Fold and function of their catalytic domains," *Biochimica et Biophysica Acta - Molecular Cell Research*, vol. 1803, no. 1. Elsevier, pp. 20–28, 01-Jan-2010.

[18] R. E. Vandenbroucke and C. Libert, "Is there new hope for therapeutic matrix metalloproteinase inhibition?," *Nature Reviews Drug Discovery*, vol. 13, no. 12. Nature Publishing Group, pp. 904–927, 11-Dec-2014.

[19] T. Eguchi *et al.*, "Organoids with cancer stem cell-like properties secrete exosomes and HSP90 in a 3D nanoenvironment," *PLoS One*, vol. 13, no. 2, Feb. 2018.

[20] Y. Okusha *et al.*, "Extracellular Oncosomes Rich in Moonlighting Metalloproteinase (MMP3) Are Transmissive, Pro-Tumorigenic, and Induces Cellular Communication Network Factor 2 (CCN2/CTGF): CRISPR against Cancer," Feb. 2020.

[21] Y. Okusha *et al.*, "The intranuclear PEX domain of MMP involves proliferation, migration, and metastasis of aggressive adenocarcinoma cells," *J. Cell. Biochem.*, vol. 119, no. April, pp. 1–14, Sep. 2018.

[22] T. Eguchi and E. A. Taha, "Extracellular Vesicle-associated Moonlighting Proteins : HSP and Metalloprteinases," pp. 1–12.

[23] Y. Namba *et al.*, "Depletion of lipid efflux pump ABCG1 triggers the intracellular accumulation of extracellular vesicles and reduces aggregation and tumorigenesis of metastatic cancer cells," *Front. Oncol.*, vol. 8, no. OCT, pp. 1–16, 2018.

[24] C. Sogawa *et al.*, "A Reporter System Evaluates Tumorigenesis, Metastasis, β-catenin/MMP Regulation, and Druggability," *Tissue Eng. - Part A*, vol. 25, no. 19–20, pp. 1413–1425, Oct. 2019.

[25] C. Sogawa *et al.*, "Antiparkinson Drug Benztropine Suppresses Tumor Growth, Circulating Tumor Cells, and Metastasis by Acting on SLC6A3/DAT and Reducing STAT3," *Cancers (Basel).*, vol. 12, no. 2, p. 523, Feb. 2020.

[26] Y. Yoshii *et al.*, "The use of nanoimprinted scaffolds as 3D culture models to facilitate spontaneous tumor cell migration and well-regulated spheroid formation," *Biomaterials*, vol. 32, no. 26, pp. 6052–6058, Sep. 2011.

[27] R. Edmondson, J. J. Broglie, A. F. Adcock, and L. Yang, "Three-dimensional cell culture systems and their applications in drug discovery and cell-based biosensors," *Assay and Drug Development Technologies*, vol. 12, no. 4. Mary Ann Liebert Inc., pp. 207–218, 01-May-2014.

[28] D. Lv, Z. Hu, L. Lu, H. Lu, and X. Xu, "Three-dimensional cell culture: A powerful tool in tumor research and drug discovery," *Oncology Letters*, vol. 14, no. 6. Spandidos Publications, pp. 6999–7010, 01-Dec-2017.

[29] K. Duval *et al.*, "Modeling physiological events in 2D vs. 3D cell culture," *Physiology*, vol. 32, no. 4. American Physiological Society, pp. 266–277, 14-Jun-2017.

[30] L. G. Griffith and M. A. Swartz, "Capturing complex 3D tissue physiology in vitro," *Nature Reviews Molecular Cell Biology*, vol. 7, no. 3. Nature Publishing Group, pp. 211–224, Mar-2006.

[31] F. Hirschhaeuser, H. Menne, C. Dittfeld, J. West, W. Mueller-Klieser, and L. A. Kunz-Schughart, "Multicellular tumor spheroids: An underestimated tool is catching up again," *J. Biotechnol.*, vol. 148, no. 1, pp. 3–15, Jul. 2010.

[32] K. Arai *et al.*, "A novel high-Throughput3D screening system for EMT inhibitors: A pilot screening discovered the EMT inhibitory activity of CDK2 inhibitor SU9516," *PLoS One*, vol. 11, no. 9, pp. 1–18, Sep. 2016.

[33] M. Elsayed and O. M. Merkel, "Nanoimprinting of topographical and 3D cell culture scaffolds," *Nanomedicine*, vol. 9, no. 2. Future Medicine Ltd., pp. 349–366, 2014.

[34] A. Yoshimura *et al.*, "Generation of a novel transgenic rat model for tracing extracellular vesicles in body fluids.," *Sci. Rep.*, vol. 6, p. 31172, Aug. 2016.

[35] Y. J. Piao, H. S. Kim, and W. K. Moon, "Noninvasive Photoacoustic Imaging of Dendritic Cell Stimulated with Tumor Cell-Derived Exosome.," *Mol. imaging Biol.*, Aug. 2019.

[36] M. P. Zaborowski *et al.*, "Methods for Systematic Identification of Membrane Proteins for Specific Capture of Cancer-Derived Extracellular Vesicles," *Cell Rep.*, vol. 27, no. 1, pp. 255--268.e6, 2019.

[37] C. P. Lai *et al.*, "multiplexed reporters," *Nat. Commun.*, vol. 6, no. May, pp. 1–12, 2015.

[38] W. Xu, "PSD-95-like membrane associated guanylate kinases (PSD-MAGUKs) and synaptic plasticity," *Current Opinion in Neurobiology*, vol. 21, no. 2. Elsevier Current Trends, pp. 306–312, 01-Apr-2011.

[39] C. Verpelli, M. J. Schmeisser, C. Sala, and T. M. Boeckers, "Scaffold proteins at the postsynaptic density," *Adv. Exp. Med. Biol.*, vol. 970, pp. 29–61, 2012.

[40] G. Triola, H. Waldmann, and C. Hedberg, "Chemical biology of lipidated proteins," *ACS Chemical Biology*, vol. 7, no. 1. American Chemical Society, pp. 87–99, 20-Jan-2012.

[41] M. X. Zuber, S. M. Strittmatter, and M. C. Fishman, "A membrane-targeting signal in the amino terminus of the neuronal protein GAP-43," *Nature*, vol. 341, no. 6240, pp. 345–348, 1989.

[42] D. A. Zacharias, J. D. Violin, A. C. Newton, and R. Y. Tsien, "Partitioning of lipid-modified monomeric GFPs into membrane microdomains of live cells," *Science (80-.).*, vol. 296, no. 5569, pp. 913–916, May 2002.

[43] S. Maacha *et al.*, "Extracellular vesicles-mediated intercellular communication: roles in the tumor microenvironment and anti-cancer drug resistance," *Mol. Cancer*, vol. 18, no. 1, Mar. 2019.

[44] T. Eguchi *et al.*, "Novel Transcription Factor-Like Function of Human Matrix Metalloproteinase 3 Regulating the CTGF/CCN2 Gene," *Mol. Cell. Biol.*, vol. 28, no. 7, pp. 2391–2413, Apr. 2008.

[45] T. Eguchi *et al.*, "Novel transcription-factor-like function of human matrix metalloproteinase 3 regulating the CTGF/CCN2 gene.," *Mol. Cell. Biol.*, vol. 28, no. 7, pp. 255–264, Apr. 2008.

[46] T. Eguchi, S. K. Calderwood, M. Takigawa, S. Kubota, and K. I. Kozaki, "Intracellular MMP3 Promotes HSP Gene Expression in Collaboration With Chromobox Proteins," *J. Cell. Biochem.*, vol. 118, no. 1, pp. 43–51, Jan. 2017.

[47] A. R. Nelson, B. Fingleton, M. L. Rothenberg, and L. M. Matrisian, "Matrix metalloproteinases:

biologic activity and clinical implications.," *J. Clin. Oncol.*, vol. 18, no. 5, pp. 1135–1149, Mar. 2000.

[48] O. J. Kaasbøll *et al.*, "Connective tissue growth factor (CCN2) is a matricellular preproprotein controlled by proteolytic activation," *J. Biol. Chem.*, vol. 293, no. 46, pp. 17953–17970, Sep. 2018.

[49] G. Hashimoto, I. Inoki, Y. Fujii, T. Aoki, E. Ikeda, and Y. Okada, "Matrix metalloproteinases cleave connective tissue growth factor and reactivate angiogenic activity of vascular endothelial growth factor 165," *J. Biol. Chem.*, vol. 277, no. 39, pp. 36288–36295, Sep. 2002.

[50] J. L. Fowlkessp, J. Enghildfl, K. O. Suzukill, and H. Nagasell, "THE JOURNAL OF BIOLEICAL CHEMISTRY Matrix Metalloproteinases Degrade Insulin-like Growth Factor-binding Protein-3 in Dermal Fibroblast Cultures*," 1994.

[51] M. Suzuki, G. Raab, M. A. Moses, C. A. Fernandez, and M. Klagsbrun, "Matrix metalloproteinase-3 releases active heparin-binding EGF-like growth factor by cleavage at a specific juxtamembrane site.," *J. Biol. Chem.*, vol. 272, no. 50, pp. 31730–31737, Dec. 1997.

[52] E. Levi, R. Fridman, H. Q. Miao, Y. S. Ma, A. Yayon, and I. Vlodavsky, "Matrix metalloproteinase 2 releases active soluble ectodomain of fibroblast growth factor receptor 1.," *Proc. Natl. Acad. Sci. U. S. A.*, vol. 93, no. 14, pp. 7069–7074, Jul. 1996.

[53] A. Ito *et al.*, "Degradation of interleukin 1beta by matrix metalloproteinases.," *J. Biol. Chem.*, vol. 271, no. 25, pp. 14657–14660, Jun. 1996.

[54] H. Haro, H. C. Crawford, B. Fingleton, K. Shinomiya, D. M. Spengler, and L. M. Matrisian, "Matrix metalloproteinase-7-dependent release of tumor necrosis factor-alpha in a model of herniated disc resorption.," *J. Clin. Invest.*, vol. 105, no. 2, pp. 143–150, Jan. 2000.

[55] F. Le Naour and M. Zoller, "The tumor antigen epcam: Tetraspanins and the tight junction protein claudin-7, new partners, new functions," *Frontiers in Bioscience*, vol. 13, no. 15. Front Biosci, pp. 5847–5865, 01-May-2008.

[56] S. Charrin, S. Manié, M. Oualid, M. Billard, C. Boucheix, and E. Rubinstein, "Differential stability of tetraspanin/tetraspanin interactions: Role of palmitoylation," *FEBS Lett.*, vol. 516, no. 1–3, pp. 139–144, Apr. 2002.

[57] X. Yang, O. V. Kovalenko, W. Tang, C. Claas, C. S. Stipp, and M. E. Hemler, "Palmitoylation supports assembly and function of integrin-tetraspanin complexes," *J. Cell Biol.*, vol. 167, no. 6, pp. 1231–1240, Dec. 2004.

[58] M. Durcin *et al.*, "Characterisation of adipocyte-derived extracellular vesicle subtypes identifies distinct protein and lipid signatures for large and small extracellular vesicles.," *J. Extracell. vesicles*, vol. 6, no. 1, p. 1305677, 2017.

[59] L. Jimenez *et al.*, "Quantitative Proteomic Analysis of Small and Large Extracellular Vesicles (EVs) Reveals Enrichment of Adhesion Proteins in Small EVs," *J. Proteome Res.*, vol. 18, no. 3, pp. 947–959, Mar. 2019.

[60] I. Parolini *et al.*, "Microenvironmental pH is a key factor for exosome traffic in tumor cells," *J. Biol. Chem.*, vol. 284, no. 49, pp. 34211–34222, Dec. 2009.

[61] K. J. Svensson *et al.*, "Exosome uptake depends on ERK1/2-heat shock protein 27 signaling and lipid raft-mediated endocytosis negatively regulated by caveolin-1," *J. Biol. Chem.*, vol. 288, no. 24, pp. 17713–17724, Jun. 2013.

[62] A. E. Morelli *et al.*, "Endocytosis, intracellular sorting, and processing of exosomes by dendritic cells," *Blood*, vol. 104, no. 10, pp. 3257–3266, Nov. 2004.

[63] A. Nanbo, E. Kawanishi, R. Yoshida, and H. Yoshiyama, "Exosomes Derived from Epstein-Barr Virus-Infected Cells Are Internalized via Caveola-Dependent Endocytosis and Promote Phenotypic Modulation in Target Cells," *J. Virol.*, vol. 87, no. 18, pp. 10334–10347, Sep. 2013.

[64] D. Fitzner *et al.*, "Selective transfer of exosomes from oligodendrocytes to microglia by macropinocytosis," *J. Cell Sci.*, vol. 124, no. 3, pp. 447–458, Feb. 2011.

[65] D. Feng *et al.*, "Cellular internalization of exosomes occurs through phagocytosis," *Traffic*, vol. 11, no. 5, pp. 675–687, May 2010.

[66] C. Escrevente, S. Keller, P. Altevogt, and J. Costa, "Interaction and uptake of exosomes by ovarian cancer cells," *BMC Cancer*, vol. 11, Mar. 2011.

[67] V. Dolo, A. Ginestra, D. Cassara, G. Ghersi, H. Nagase, and M. L. Vittorelli, "Shed membrane vesicles and selective localization of gelatinases and MMP-9/TIMP-1 complexes.," *Ann. N. Y. Acad. Sci.*, vol. 878, pp. 497–499, Jun. 1999.

[68] G. Taraboletti, S. D'Ascenzo, P. Borsotti, R. Giavazzi, A. Pavan, and V. Dolo, "Shedding of the matrix metalloproteinases MMP-2, MMP-9, and MT1-MMP as membrane vesicle-associated components by endothelial cells," *Am. J. Pathol.*, vol. 160, no. 2, pp. 673–680, Feb. 2002.

[69] M. Belhocine, T. Gernigon-Spychalowicz, M. P. Jacob, Y. Benazzoug, and J. M. Exbrayat, "Immunoexpression of gelatinase (MMP-2 and MMP-9) in the seminal vesicles and ventral prostate of Libyan jird (Meriones libycus) during the seasonal cycle of reproduction," *Histol. Histopathol.*, vol. 25, no. 5, pp. 619–636, May 2010.

[70] M. Shimoda and R. Khokha, "Proteolytic factors in exosomes," *Proteomics*, vol. 13, no. 10–11. John Wiley & Sons, Ltd, pp. 1624–1636, 01-May-2013.

[71] A. T. Reiner *et al.*, "EV-Associated MMP9 in High-Grade Serous Ovarian Cancer Is Preferentially Localized to Annexin V-Binding EVs.," *Dis. Markers*, vol. 2017, p. 9653194, 2017.

[72] J. McCready, J. D. Sims, D. Chan, and D. G. Jay, "Secretion of extracellular hsp90α via exosomes increases cancer cell motility: A role for plasminogen activation," *BMC Cancer*, vol. 10, p. 294, Jun. 2010.

[73] J. D. Sims, J. McCready, and D. G. Jay, "Extracellular Heat Shock Protein (Hsp)70 and Hsp90α Assist in Matrix Metalloproteinase-2 Activation and Breast Cancer Cell Migration and Invasion," *PLoS One*, vol. 6, no. 4, p. e18848, Apr. 2011.

[74] K. Ono *et al.*, "HSP-enriched properties of extracellular vesicles involve survival of metastatic oral cancer cells," *J. Cell. Biochem.*, vol. 119, no. 9, pp. 7350–7362, Sep. 2018.

[75] T. Eguchi *et al.*, "Regulatory Roles of HSP90-Rich Extracellular Vesicles," no. December, Springer, Cham, 2019, pp. 3–17.

[76] W. Jin and J. Wang, "Adipocyte-derived exosomes promote lung cancer metastasis byincreasing MMP9 activity via transferring MMP3 to lung cancer cells," *Eur. Respir. J.*, vol. 50, no. suppl 61, 2017.

[77] H. Nagaset and J. F. Woessner, "Matrix metalloproteinases," *Journal of Biological Chemistry*, vol. 274, no. 31. American Society for Biochemistry and Molecular Biology, pp. 21491–21494, 30-Jul-1999.

[78] L. Ravanti and V. M. Kähäri, "Matrix metalloproteinases in wound repair (review).," *International journal of molecular medicine*, vol. 6, no. 4. Spandidos Publications, pp. 391–407, 01-Oct-2000.

[79] K. Sakata *et al.*, "Establishment and characterization of high- and low-lung-metastatic cell lines derived from murine colon adenocarcinoma 26 tumor line.," *Jpn. J. Cancer Res.*, vol. 87, no. 1, pp. 78–85, Jan. 1996.